ESD-TR-89-235

Technical Report
870

Low-Sidelobe Phased Array Antenna Characteristics Using the Planar Near-Field Scanning Technique: Theory and Experiment

A.J. Fenn
H.M. Aumann
F.G. Willwerth

14 February 1990

Lincoln Laboratory
MASSACHUSETTS INSTITUTE OF TECHNOLOGY
LEXINGTON, MASSACHUSETTS

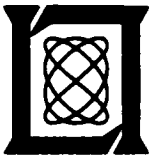

Prepared for the Department of the Air Force under Contract F19628-90-C-0002.

This report is based on studies performed at Lincoln Laboratory, a center for research operated by Massachusetts Institute of Technology. The work was sponsored by the Department of the Air Force under Contract F19628-90-C-0002.

The ESD Public Affairs Office has reviewed this report, and it is releasable to the National Technical Information Service, where it will be available to the general public, including foreign nationals.

This technical report has been reviewed and is approved for publication.

FOR THE COMMANDER

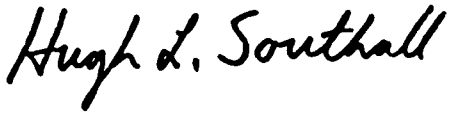

Hugh L. Southall, Lt. Col., USAF
Chief, ESD Lincoln Laboratory Project Office

MASSACHUSETTS INSTITUTE OF TECHNOLOGY
LINCOLN LABORATORY

LOW-SIDELOBE PHASED ARRAY ANTENNA CHARACTERISTICS USING THE PLANAR NEAR-FIELD SCANNING TECHNIQUE: THEORY AND EXPERIMENT

A.J. FENN
H.M. AUMANN
F.G. WILLWERTH
Group 61

TECHNICAL REPORT 870

14 FEBRUARY 1990

LEXINGTON MASSACHUSETTS

ABSTRACT

Characteristics of a low-sidelobe phased array antenna are investigated using the technique of planar near-field scanning. The theory associated with the planar near-field scanning technique, with and without probe compensation, is reviewed and an application of the theory is made. The design of an experimental low-sidelobe phased array antenna consisting of monopole elements which are corporate-fed using high precision transmit/receive modules is described. Accurate array radiation patterns are obtained both theoretically and experimentally using centerline scanning at less than one wavelength distance from the antenna. The effects of the antenna probe on the array near-field pattern, plane-wave spectrum, and far-field pattern are demonstrated theoretically using a method of moments numerical simulation. Comparisons of the array theoretical near-zone electric field and array received voltage due to a V-dipole near-field transmitting probe are made. It is shown that a V-dipole theoretical probe antenna can accurately model a practical near-field measurement probe consisting of an open-ended rectangular waveguide surrounded with anechoic material.

ACKNOWLEDGEMENTS

The authors wish to express their gratitude to S.E. French for running the numerical simulations and plotting the data.

TABLE OF CONTENTS

LIST OF ILLUSTRATIONS

LIST OF ILLUSTRATIONS
(Continued)

1. INTRODUCTION

The planar near-field scanning technique has seen considerable use during recent years for determining the far-field radiation patterns of antennas [1-4]. The technique is particularly well suited for evaluating the performance of low-sidelobe planar phased array antennas [5]. In a phased array antenna, low sidelobes are achieved using appropriate aperture amplitude taper together with precision element weighting and array calibration. To evaluate the performance of these antennas, high quality near-field measurements are often desirable. The near field is measured typically using a low-gain antenna probe which is moved to a regular grid of points on a planar surface as depicted in Figure 1-1.

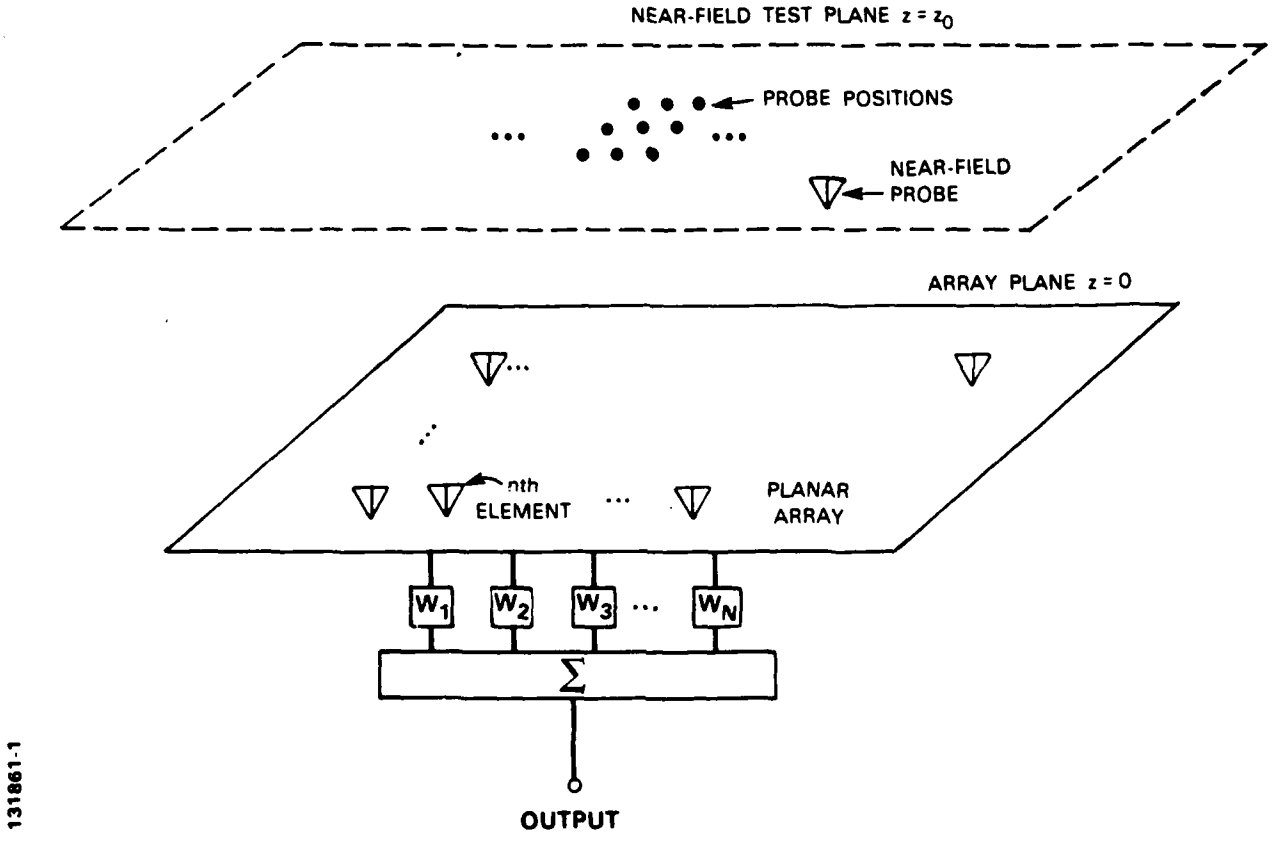

Figure 1-1. Phased array antenna and near-field test plane.

The probe can be used either to transmit or receive the desired RF signal (usually a CW tone). After collecting the near-field data, a general-purpose computer is used to mathematically transform the data, by means of the antenna plane-wave spectrum, to a far-field pattern. The plane-wave spectrum is essentially the Fourier transform of the antenna aperture illumination and

consists of radiating and evanescent plane waves. The radiating plane waves reach the antenna far-field region and, thus, contribute to the far-field pattern. For a phased array antenna, an example of an evanescent plane wave is a nonpropagating grating lobe.

Planar near-field measurements are commonly performed in the radiating near-field region [3]. In this region (typically two to ten wavelengths from the test antenna aperture), the evanescent contributions of the near field are sufficiently attenuated so that conventional one-half wavelength data sample spacing can be used. It is well known that as the near-field test distance decreases, the near-field data sample spacing tends to decrease in order to take into account the increase which occurs in the evanescent component [6]. Data collection at a distance of approximately one wavelength or less is implemented in what has been referred to as the reactive or evanescent near-field region [3]. The effect of the evanescent near field on the required sample spacing is a function of the aperture illumination and aperture diameter as has been addressed theoretically by Wang [7]. For a phased array antenna, effects of the near-field probe on the near-field data, plane-wave spectrum, and transformed far-field pattern have not previously been theoretically quantified.

To better understand phased array characteristics as determined by the planar near-field scanning technique, two theoretical models are investigated. Both theories are intended to apply in the evanescent and radiating near-field region. The first is referred to in this report as the field point theory, which is the same as near-field scanning without probe compensation. Here, the tangential electric field component radiated by an antenna is computed at a series of near-field points. The second theory is referred to as the dipole probe theory where the received voltage at a V-dipole near-field antenna probe is computed at a series of probe positions. This is an application of the probe-compensated near-field scanning technique. Both theoretical models include the effects of array polarization and mutual coupling through the use of the method of moments, as described in the next chapter. The theory is applied to the case of a monopole phased array antenna. The design of a low-sidelobe corporate-fed linear phased array of monopole antenna elements is discussed in chapter 3. In chapter 4, a brief discussion of the near-field measurements system is given. Theoretical and experimental results are presented in chapter 5. Centerline scanning at less than one wavelength distance from the antenna under test is used to obtain the plane-wave spectrum and far-field pattern. The effects of the probe on the near-field theoretical data, plane-wave spectrum, and transformed far-field pattern are demonstrated. It is shown that a thin-wire V-dipole theoretical probe antenna can accurately model an experimental near-field measurement probe which consists of a rectangular waveguide surrounded with anechoic material.

2. THEORY

2.1 PLANAR NEAR-FIELD SCANNING FORMULATION

The purpose of this section is to briefly review the theory for determining far-field radiation patterns from measured or theoretical near-field data. The formulation differs somewhat from that which is presented in [1] with respect to the notation and the test antenna orientation in the reference rectangular coordinate system. To begin, let the time-harmonic electric field radiated from an aperture be denoted by $\boldsymbol{E}(x, y, z)$ and let the aperture be located on the xy plane as shown in Figure 2-1(a).

At any distance z in front of the aperture the electric field can be represented as a superposition of plane waves [1,8,9]. In general, these plane waves can be evanescent or propagating depending on the distance from the aperture.

From Maxwell's equations in free space (described by permittivity ϵ_o and permeability μ_o) and a vector identity, the vector wave equation is expressed as

$$\nabla^2 \boldsymbol{E} + k^2 \boldsymbol{E} = 0$$

where $k = \omega\sqrt{\mu_o \epsilon_o} = 2\pi/\lambda$ is the propagation constant or wavenumber, λ is the wavelength, and ∇^2 is the Laplacian operator. A trial solution to the wave equation, for outgoing waves, with the $e^{j\omega t}$ time variation suppressed is of the form

$$\boldsymbol{E}(x, y, z) = \boldsymbol{A}(\boldsymbol{k}) e^{-j\boldsymbol{k}\cdot\boldsymbol{r}} \tag{2.1}$$

where

$$\boldsymbol{r} = x\hat{\boldsymbol{x}} + y\hat{\boldsymbol{y}} + z\hat{\boldsymbol{z}}$$

is the observation position vector,

$$\boldsymbol{k} = k_x\hat{\boldsymbol{x}} + k_y\hat{\boldsymbol{y}} + k_z\hat{\boldsymbol{z}}$$

is the propagation vector, and as is depicted in Figure 2-1(b)

$$\boldsymbol{A} = A_x\hat{\boldsymbol{x}} + A_y\hat{\boldsymbol{y}} + A_z\hat{\boldsymbol{z}} \tag{2.2}$$

is the commonly referred to complex plane-wave amplitude function or plane-wave spectrum. The wavenumber components in terms of spherical coordinates are

$$k_x = k \sin\theta \cos\phi \tag{2.3}$$

$$k_y = k \sin\theta \sin\phi \tag{2.4}$$

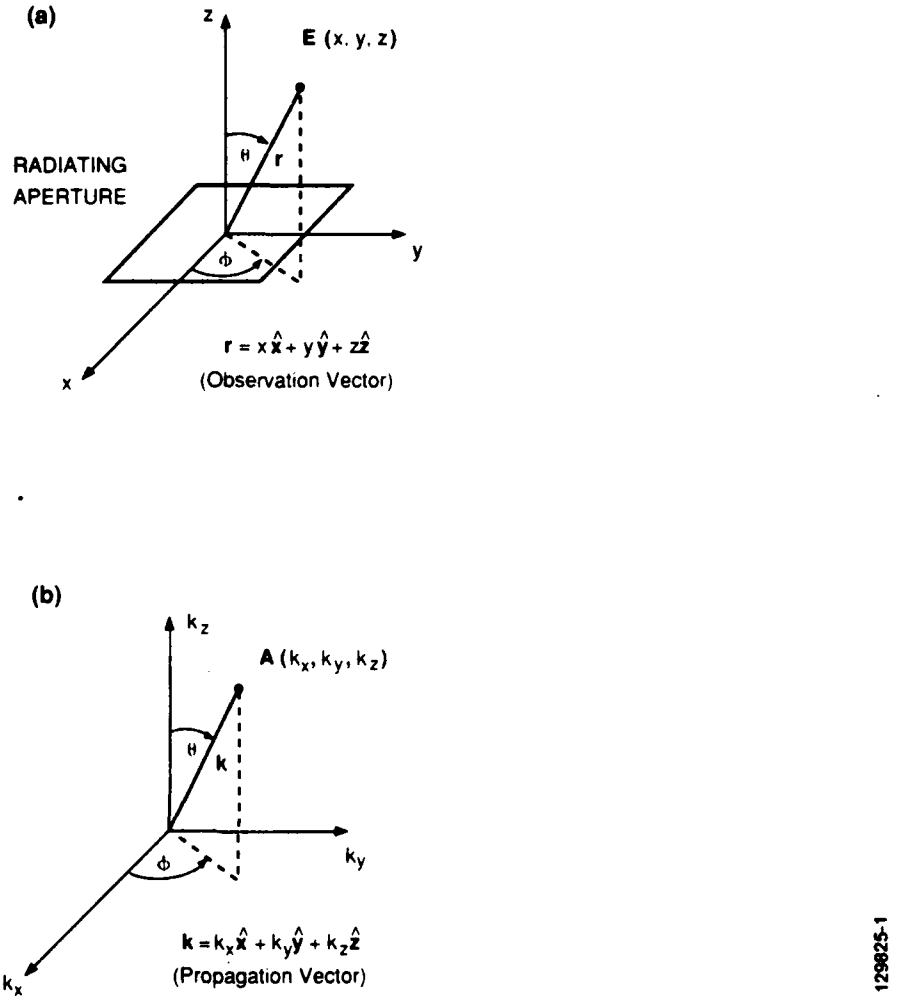

Figure 2-1. Coordinate systems for describing (a) electric field and (b) plane-wave spectrum.

$$k_z = k \cos\theta. \tag{2.5}$$

From Equations (2.3) through (2.5) observe that

$$k^2 = k_x^2 + k_y^2 + k_z^2. \tag{2.6}$$

In Equation (2.6), k_x and k_y are chosen to be the independent variables with k_z being the dependent variable, such that

$$k_z = \begin{cases} \sqrt{k^2 - k_x^2 - k_y^2} & k_x^2 + k_y^2 \leq k^2 \\ -j\sqrt{k_x^2 + k_y^2 - k^2} & k_x^2 + k_y^2 > k^2. \end{cases}$$

Only two components of $\boldsymbol{A}$ are independent, A_x and A_y, with A_z chosen to be the dependent variable. Now since $\nabla \cdot \boldsymbol{E} = 0$, from Equations (2.1) and (2.2) it is readily shown that

$$A_z(k_x, k_y) = -\frac{1}{k_z}(k_x A_x + k_y A_y).$$

The general solution for $\boldsymbol{E}$ can be expressed as a linear combination of $\boldsymbol{A}$ over all values of k_x and k_y as

$$\boldsymbol{E}(x, y, z) = \int_{-\infty}^{\infty} \int_{-\infty}^{\infty} \boldsymbol{A}(k_x, k_y) e^{-j\boldsymbol{k}\cdot\boldsymbol{r}} dk_x dk_y.$$

2.1.1 Test Antenna Has Known Electric Field

If the tangential electric field $\boldsymbol{E}_t$ is known over a planar surface at $z = z_o$, the plane-wave spectrum can be determined from the inverse Fourier transform relationship

$$\boldsymbol{A}(k_x, k_y) = \frac{1}{4\pi^2} \int_{-\infty}^{\infty} \int_{-\infty}^{\infty} \boldsymbol{E}_t(x, y, z_o) e^{j\boldsymbol{k}\cdot\boldsymbol{r}} dx dy.$$

Specifically, for $\boldsymbol{E}_t = E_x \hat{\boldsymbol{x}} + E_y \hat{\boldsymbol{y}}$ the components of $\boldsymbol{A}$ are

$$A_x(k_x, k_y) = e^{jk_z z_o} A_x(k_x, k_y, z_o)$$

$$A_y(k_x, k_y) = e^{jk_z z_o} A_y(k_x, k_y, z_o)$$

where

$$A_x(k_x, k_y, z_o) = \frac{1}{4\pi^2} \int_{-\infty}^{\infty} \int_{-\infty}^{\infty} E_x(x, y, z_o) e^{j(k_x x + k_y y)} dx dy \tag{2.7}$$

$$A_y(k_x, k_y, z_o) = \frac{1}{4\pi^2} \int_{-\infty}^{\infty} \int_{-\infty}^{\infty} E_y(x, y, z_o) e^{j(k_x x + k_y y)} dx dy \tag{2.8}$$

are the plane-wave spectrum components for the measurement plane. As suggested in Figure 1-1, the infinite integrals in Equations (2.7) and (2.8) are truncated according to the near-field scan length. For uniformly spaced near-field data, the resulting finite integrals are evaluated efficiently using the fast Fourier transform (FFT) algorithm.

From Rhodes [10], in the far field of the antenna the electric field can be written in terms of the plane-wave spectrum as

$$\boldsymbol{E}(r,\theta,\phi) = j2\pi k\cos\theta\frac{e^{-jkr}}{r}\boldsymbol{A}(k_x,k_y). \tag{2.9}$$

To obtain E_θ and E_ϕ components a standard conversion from rectangular components to spherical components is made.

2.1.2 Test Antenna Has Known Received Voltage: Near-Field Probe Pattern Compensation

In practice the near-field measured data are collected by utilizing a movable antenna probe. The probe is assumed here to be linearly polarized and is used as a transmitting source. In this case, the test antenna received voltage is known, rather than its electric field. At each near-field position, two probe orientations are in general required—one where the probe is $\hat{x}$-polarized and the other where the probe is $\hat{y}$-polarized. Let the far-zone electric field vector pattern of the near-field probe with x,y orientations in free space be expressed as

$$\boldsymbol{e}^x(\theta,\phi) = \hat{\theta}e^x_\theta(\theta,\phi) + \hat{\phi}e^x_\phi(\theta,\phi) \tag{2.10}$$

$$\boldsymbol{e}^y(\theta,\phi) = \hat{\theta}e^y_\theta(\theta,\phi) + \hat{\phi}e^y_\phi(\theta,\phi). \tag{2.11}$$

It is further assumed that the probe pattern is not affected by the presence of the test antenna and that the probe far-field pattern can be obtained by conventional far-field measurements.

Next, let the test antenna far-field pattern be given by

$$\boldsymbol{E}(\theta,\phi) = \hat{\theta}E_\theta(\theta,\phi) + \hat{\phi}E_\phi(\theta,\phi). \tag{2.12}$$

In Equation (2.12), E_θ and E_ϕ represent the two desired components of the antenna under test. They will be determined in what follows by solving two simultaneous equations.

Let $\boldsymbol{a}^x, \boldsymbol{a}^y$ denote the probe plane-wave spectrum for $\hat{x}$-, $\hat{y}$-polarized probe orientations, respectively. The received voltage at the array output, for a near-field transmitting probe at position (x,y,z_o), is given as [1]

$$v^x(x,y,z_o) = \frac{8\pi^2}{\omega\mu}\int_{-\infty}^{\infty}\int_{-\infty}^{\infty} k_z\boldsymbol{A}(k_x,k_y)\cdot\boldsymbol{a}^x(k_x,k_y)e^{-j\boldsymbol{k}\cdot\boldsymbol{r}_o}dk_xdk_y \tag{2.13}$$

$$v^y(x,y,z_o) = \frac{8\pi^2}{\omega\mu}\int_{-\infty}^{\infty}\int_{-\infty}^{\infty} k_z\boldsymbol{A}(k_x,k_y)\cdot\boldsymbol{a}^y(k_x,k_y)e^{-j\boldsymbol{k}\cdot\boldsymbol{r}_o}dk_xdk_y. \tag{2.14}$$

In words, the received voltage $v(x,y,z_o)$ is equal to the superposition over all k_x, k_y of the dot product of the test antenna plane-wave spectrum and probe plane-wave spectrum. Taking the inverse Fourier transform of Equations (2.13) and (2.14) and defining an apparent or probe-distorted plane-wave spectrum as

$$A'^x(k_x, k_y, z_0) = \frac{1}{4\pi^2}\int_{-\infty}^{\infty}\int_{-\infty}^{\infty} v^x(x, y, z_o)e^{j(k_x x + k_y y)}dxdy \tag{2.15}$$

$$A'^y(k_x, k_y, z_0) = \frac{1}{4\pi^2}\int_{-\infty}^{\infty}\int_{-\infty}^{\infty} v^y(x, y, z_o)e^{j(k_x x + k_y y)}dxdy \tag{2.16}$$

yields

$$k_z \boldsymbol{A}(k_x, k_y)\cdot \boldsymbol{a}^x = \frac{\omega\mu}{8\pi^2}e^{jk_z z_o}A'^x(k_x, k_y, z_0) \tag{2.17}$$

$$k_z \boldsymbol{A}(k_x, k_y)\cdot \boldsymbol{a}^y = \frac{\omega\mu}{8\pi^2}e^{jk_z z_o}A'^y(k_x, k_y, z_0). \tag{2.18}$$

As in Equations (2.7) and (2.8), the infinite integrals in Equations (2.15) and (2.16) are replaced by finite integrals according to the actual near-field scan lengths. Next, analogous to Equation (2.9) the probe far-zone electric field is written in terms of the probe plane-wave spectrum as

$$\boldsymbol{e}^x(r, \theta, \phi) = j2\pi k\cos\theta\frac{e^{-jkr}}{r}\boldsymbol{a}^x(k_x, k_y) \tag{2.19}$$

$$\boldsymbol{e}^y(r, \theta, \phi) = j2\pi k\cos\theta\frac{e^{-jkr}}{r}\boldsymbol{a}^y(k_x, k_y) \tag{2.20}$$

where $\boldsymbol{e}^x$,$\boldsymbol{e}^y$ denote the far-field vector patterns for the x-,y-directed probe, respectively. Substituting Equations (2.9), (2.19), and (2.20) into (2.17) and (2.18) and dropping the e^{-jkr}/r dependence as usual in the far field yields

$$\boldsymbol{E}(\theta, \phi)\cdot \boldsymbol{e}^x(\theta, \phi) = C\cos\theta e^{jk_z z_o}A'^x \tag{2.21}$$

$$\boldsymbol{E}(\theta, \phi)\cdot \boldsymbol{e}^y(\theta, \phi) = C\cos\theta e^{jk_z z_o}A'^y \tag{2.22}$$

where the constant C is given as

$$C = -\frac{k\omega\mu_0}{2}.$$

Equations (2.21) and (2.22) are solved simultaneously for the components E_θ and E_ϕ by utilizing Equations (2.10), (2.11), and (2.12) with the result

$$E_\theta = C\cos\theta e^{jk_z z_o}\frac{e_\phi^y A'^x - e_\phi^x A'^y}{\Delta} \tag{2.23}$$

$$E_\phi = C\cos\theta e^{jk_z z_o}\frac{-e_\theta^y A'^x + e_\theta^x A'^y}{\Delta}$$

where

$$\Delta = e_\theta^x e_\phi^y - e_\phi^x e_\theta^y.$$

For a $\phi = 0°$ pattern cut of a predominantly E_θ-polarized linear array antenna $A'^x \gg A'^y$. Assuming a probe with low cross-polarization characteristics (that is, $e_\phi^x \ll e_\theta^x, e_\theta^y \ll e_\theta^x$), then Equation (2.23) reduces to

$$E_\theta \approx C \cos\theta e^{jk_z z_o} \frac{A'^x}{e_\theta^x}. \tag{2.24}$$

In evaluating the plane-wave spectrum function A'^x, given by Equation (2.15), an N_x-point (including zero filling) FFT is used. Assuming the near-field sample spacing is denoted by d_x and that the unfolded FFT index is denoted by K_x, then the transform wavenumber is given by

$$k_x = \frac{2\pi(K_x - N_x/2)}{d_x N_x}. \tag{2.25}$$

The far-field angle (θ) is computed from the wavenumber k_x by the use of Equations (2.3) and (2.25).

2.2 MONOPOLE PHASED ARRAY NEAR-FIELD MODELING USING THE METHOD OF MOMENTS

In the method of moments [11], boundary conditions are used to find the antenna response to a given excitation. The excitation here is the amplitude and phase incident at each element of the phased array. Due to mutual coupling or the mutual impedance between array elements, the actual illumination achieved will be different from that which is theoretically desired.

It is assumed that there is one unknown complex current function per element of the array. A piecewise-sinusoidal current distribution is used as the moment method basis and testing functions. Since the basis functions and testing functions are the same, this is known as a Galerkin's formulation. For a piecewise-sinusoidal Galerkin's moment method formulation, the mutual impedance between array elements is readily computed [12]. In this report, the array elements are assumed to be resonant monopoles and, from a previous study, it is known that one unknown per element is adequate for pattern computation [13].

2.2.1 Field Point Approach

The geometry for a finite array of monopoles over an infinite ground plane is shown in Figure 2-2(a). Standard spherical coordinate angles (θ, ϕ) are used to describe the observation position for far-field pattern computation. The ground plane is located in the $z = 0$ plane and the monopoles are $\hat{z}$-polarized. Using image theory, the ground plane can be removed from the

analysis. For a monopole array, an equivalent dipole array results [Figure 2-2(b)]. From far-field theory, the monopole radiates (or receives) only the E_θ electric field component. The nth array element is located at the position (x_n, y_n), and the electric current which flows along the wire is assumed to be of the form

$$i_n(z) = i_n \frac{\sin[k(l - |z|)]}{\sin(kl)} \tag{2.26}$$

where i_n is the complex terminal current, l is the dipole half-length (monopole length), and $k = 2\pi/\lambda$ is the propagation constant. For the nth array element, the tangential near-field components on the plane $z = z_o$ are expressed as

$$E_{nx}(x, y, z_o) = E_{n\rho'} \cos\phi'$$

$$E_{ny}(x, y, z_o) = E_{n\rho'} \sin\phi'$$

where [14]

$$E_{n\rho'} = \frac{30ji_n}{\rho' \sin(kl)}(e^{-jkr_1}\cos\theta_1 + e^{-jkr_2}\cos\theta_2 - 2\cos(kl)e^{-jkr_o}\cos\theta_o)$$

is the radial component of the electric field in cylindrical coordinates and where, r_o, r_1, r_2, ρ', θ_o, θ_1, and θ_2 are defined in Figure 2-2(b) and $\phi' = \tan^{-1}[(y - y_n)/(x - x_n)]$. To compute the antenna near field including array mutual coupling effects, it is necessary to determine the array terminal currents defined above using the method of moments.

Let $\boldsymbol{Z}$ represent the mutual impedance matrix for the equivalent dipole array. Referring to Figure 2-3(a), $\boldsymbol{Z}$ is expressed as

$$\boldsymbol{Z} = \boldsymbol{Z}^{o.c.} + Z_L \boldsymbol{I} \tag{2.27}$$

where $\boldsymbol{Z}^{o.c.}$ is the open-circuit mutual impedance matrix for the array, $\boldsymbol{I}$ is the identity matrix, and Z_L is the load impedance.

The mutual impedance Z_{mn} between two identical parallel elements is a function only of the length of the elements and the element spacing. The self-impedance Z_{mm} of the array elements is taken to be equal to the mutual impedance between two thin elements separated by one wire radius.

Define $\boldsymbol{v}$ as the voltage excitation matrix of the array. The array element terminal currents, denoted $\boldsymbol{i}$, are then found by solving the system of equations written in matrix form as

$$\boldsymbol{v} = \boldsymbol{Z} \cdot \boldsymbol{i}. \tag{2.28}$$

The nth element of the voltage excitation matrix for a phased array antenna is given by

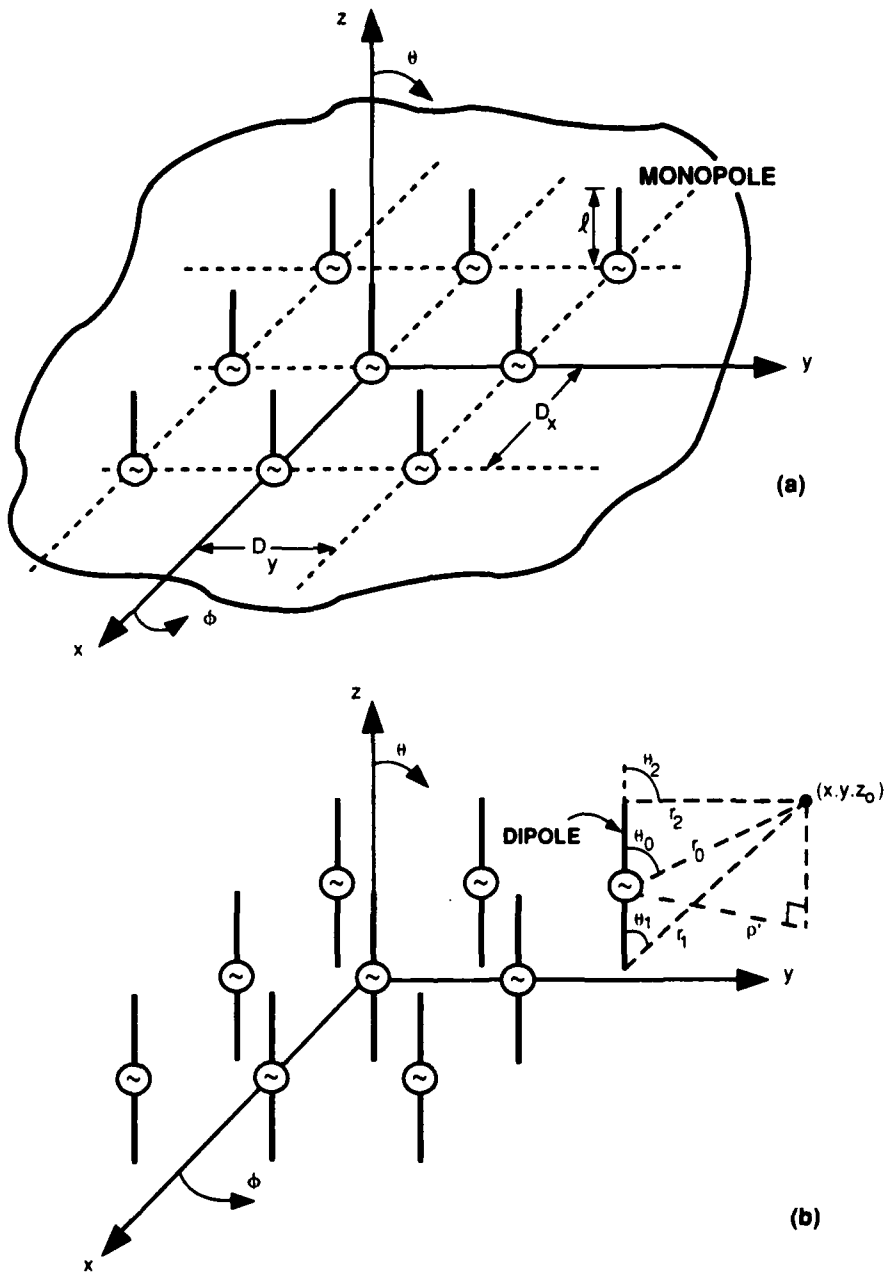

Figure 2-2. Geometry for finite array antennas: (a) monopole array over ground plane and (b) equivalent dipole array with ground plane removed and monopole images included.

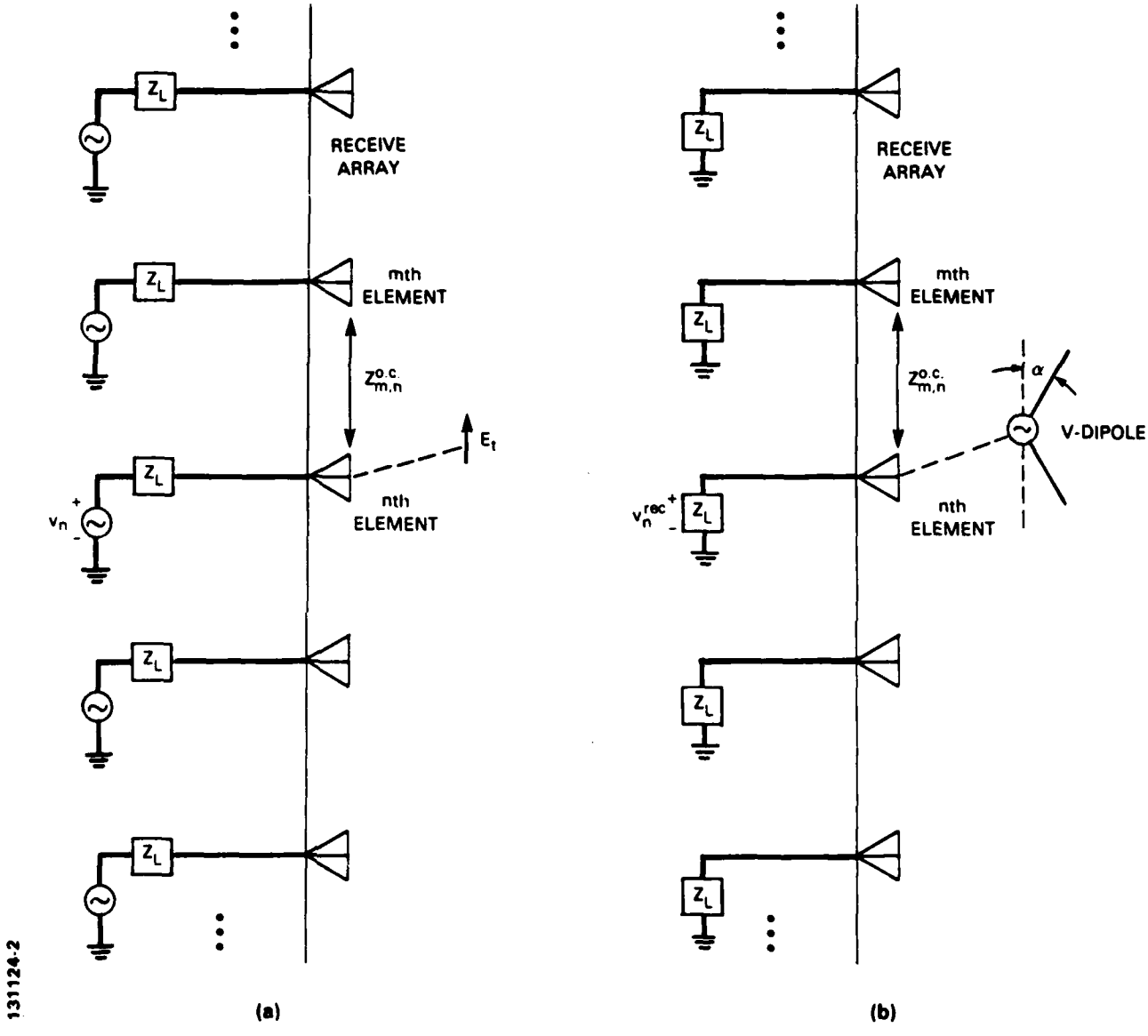

Figure 2-3. Near-field modeling for phased array antenna: (a) field point theory approach where the array is transmitting and the near-zone electric field is computed and (b) dipole probe theory where a V-dipole antenna is transmitting and the voltage received by the array is computed.

$$v_n = A_n e^{-j\psi_n}$$

where A_n is the amplitude illumination and

$$\psi_n = k \sin\theta_s (x_n \cos\phi_s + y_n \sin\phi_s) \tag{2.29}$$

is the phase progression which scans the main beam in the direction (θ_s, ϕ_s).

Using Equation (2.27) in (2.28), the array terminal currents are found according to

$$\boldsymbol{i} = [\boldsymbol{Z}^{o.c.} + Z_L \boldsymbol{I}]^{-1} \boldsymbol{v}$$

where $^{-1}$ means matrix inverse. Finally, the array near-zone field including mutual coupling effects is expressed by superposition as

$$E_x(x, y, z_o) = \sum_{n=1}^{N} E_{nx} \tag{2.30}$$

$$E_y(x, y, z_o) = \sum_{n=1}^{N} E_{ny}. \tag{2.31}$$

Upon evaluating Equations (2.30) and (2.31) numerically, the field point theory plane-wave spectrum, given by Equations (2.7) and (2.8), can be computed, from which the far-field pattern is determined from Equation (2.9).

Having determined the array terminal currents, the far-field pattern can, of course, be computed directly using the product of the isolated element far-field pattern and the array factor as,

$$P_\theta(\theta, \phi) = p_\theta(\theta) \sum_{n=1}^{N} i_n e^{jk \sin\theta (x_n \cos\phi + y_n \sin\phi)} \tag{2.32}$$

where

$$p_\theta(\theta) = \frac{\cos(kl \sin\theta) - \cos(kl)}{\cos\theta}$$

is the pattern of a vertical dipole. Equation (2.32) will be used later to show that a centerline near-field scan which is transformed to the far field is a close approximation to the direct far-field pattern.

2.2.2 Dipole Probe Approach

In this section, an expression for the voltage received by array antenna elements, due to a near-field radiating probe antenna, is derived. A similar formulation for the case of a far-field source is addressed in [15]. The formulation has also found use in the application of near-field adaptive nulling [16].

A V-dipole probe is selected here because its pattern shape is readily adjusted by varying the tilt angle of the dipole arms; thus, the pattern of the V-dipole can be made approximately equal to that of a practical near-field probe which is typically an open-ended waveguide. The current distribution on the V-dipole is assumed to be piecewise-sinusoidal. Consider Figure 2-3(b) which depicts the circuit model for a receive array and a source antenna. Let $v_n^{rec}(x, y, z_o)$ be the voltage received in the nth array element due to a near-field source antenna at position (x, y, z_o). The array elements are assumed to be terminated in a load impedance denoted Z_L, which in general is complex. The open-circuit mutual impedance between the mth and nth array elements is denoted by $Z_{m,n}^{o.c.}$. Similarly, the open-circuit mutual impedance between the nth array element and the near-field V-dipole source antenna is denoted $Z_{n,probe}^{o.c.}(x, y, z_o)$, which is evaluated using computer subroutines discussed in [17]. Now, $i_1, i_2, \cdots, i_n, \cdots, i_N$ are the received terminal currents for the N array elements. The received voltages are related to the terminal currents and load impedances using

$$v_n^{rec}(x, y, z_o) = -i_n^{rec}(x, y, z_o) Z_L, \quad n = 1, 2, \cdots, N. \tag{2.33}$$

Let i_t be the terminal current of the near-field source antenna. It is assumed that the array antenna does not affect the terminal current of the source antenna. This means that multiple interaction between the source antenna and array antenna is ignored. The array received voltages can be written as

$$\begin{aligned}
v_1^{rec} &= i_1^{rec} Z_{1,1}^{o.c} + i_2^{rec} Z_{1,2}^{o.c.} + \cdots + i_n^{rec} Z_{1,n}^{o.c.} + \cdots + i_N^{rec} Z_{1,N}^{o.c.} + i_t Z_{1,probe}^{o.c.}(x, y, z_o) \\
&\vdots \\
v_n^{rec} &= i_1^{rec} Z_{n,1}^{o.c} + i_{2,j}^{rec} Z_{n,2}^{o.c.} + \cdots + i_n^{rec} Z_{n,n}^{o.c.} + \cdots + i_N^{rec} Z_{n,N}^{o.c.} + i_t Z_{n,probe}^{o.c.}(x, y, z_o) \\
&\vdots \\
v_N^{rec} &= i_1^{rec} Z_{N,1}^{o.c} + i_{2,j}^{rec} Z_{N,2}^{o.c.} + \cdots + i_n^{rec} Z_{N,n}^{o.c.} + \cdots + i_N^{rec} Z_{N,N}^{o.c.} + i_t Z_{N,probe}^{o.c.}(x, y, z_o).
\end{aligned} \tag{2.34}$$

In the above equation, the term $i_t Z_{n,probe}^{o.c.}(x, y, z_o)$ is the open-circuit voltage at the nth array element due to a near-field probe at position (x, y, z_o).

Now, define

$$v_n^{o.c.}(x, y, z_o) = i_t Z_{n,probe}^{o.c.}(x, y, z_o), \tag{2.35}$$

and using Equations (2.33) and (2.35) in Equation (2.34) and rearranging terms yields

$$
\begin{aligned}
-v_1^{o.c.} &= i_1^{rec}(Z_{1,1}^{o.c.} + Z_L) + \cdots + i_n^{rec} Z_{1,n}^{o.c.} + \cdots + i_N^{rec} Z_{1,N}^{o.c.} \\
&\vdots \\
-v_n^{o.c.} &= i_1^{rec} Z_{n,1}^{o.c.} + \cdots + i_n^{rec}(Z_{n,n}^{o.c.} + Z_L) + \cdots + i_N^{rec} Z_{n,N}^{o.c.} \\
&\vdots \\
-v_N^{o.c.} &= i_1^{rec} Z_{N,1}^{o.c.} + \cdots + i_n^{rec} Z_{N,n}^{o.c.} + \cdots + i_N^{rec}(Z_{N,N}^{o.c.} + Z_L).
\end{aligned} \tag{2.36}
$$

Equation (2.36) can be written in matrix form as

$$
-\boldsymbol{v}^{o.c.} = (\boldsymbol{Z}^{o.c.} + Z_L \boldsymbol{I})\, \boldsymbol{i}^{rec} \tag{2.37}
$$

where $\boldsymbol{v}^{o.c.}$ is the array open-circuit voltage matrix, $\boldsymbol{Z}^{o.c.}$ is the array open-circuit mutual impedance matrix, $\boldsymbol{I}$ denotes the identity matrix, and $\boldsymbol{i}^{rec}$ is the array received terminal current matrix. From Equation (2.33) it is clear that

$$
\boldsymbol{i}^{rec} = -\frac{\boldsymbol{v}^{rec}}{Z_L}. \tag{2.38}
$$

Substituting Equation (2.38) in Equation (2.37) and solving for $\boldsymbol{v}^{rec}$ yields

$$
\boldsymbol{v}^{rec}(x, y, z_o) = Z_L\, (\boldsymbol{Z}^{o.c.} + Z_L \boldsymbol{I})^{-1}\, \boldsymbol{v}^{o.c.}(x, y, z_o)
$$

which gives the element received voltages. To compute the array beamformer (coherent power combiner) output, define an array weight vector, $\boldsymbol{w}$, where the nth element is given by

$$
w_n = A_n e^{-j\psi_n}
$$

with A_n being the amplitude illumination and ψ_n being the phase illumination given by Equation (2.29); thus, the complex received voltage at the array output port, due to the near-field radiating probe, is expressed as

$$
v_{output}^{rec}(x, y, z_o) = \boldsymbol{w}^{\dagger} \cdot \boldsymbol{v}^{rec}(x, y, z_o) \tag{2.39}
$$

where † means complex conjugate transpose.

To implement probe compensation for a V-dipole probe it is convenient to use a closed-form expression for the far-field radiation pattern. Using the notation of Equation (2.24), the far-field pattern of a V-dipole antenna, with arm tilt angle α and arm length l_v and having a sinusoidal current distribution of the form of Equation (2.26), is readily obtained by adding the contributions of two monopoles forming a V shape [18]. The result is

$$
\begin{aligned}
e_{\theta}^{x} = \frac{j30 i_t}{\sin(kl_v)} \Big(& \frac{e^{jkl_v \sin(\theta+\alpha)} - j\sin(\theta+\alpha)\sin(kl_v) - \cos(kl_v)}{\cos(\theta+\alpha)} \\
& + \frac{e^{-jkl_v \sin(\theta-\alpha)} + j\sin(\theta-\alpha)\sin(kl_v) - \cos(kl_v)}{\cos(\theta-\alpha)} \Big).
\end{aligned} \tag{2.40}
$$

To demonstrate the accuracy of the above closed-form expression (which assumes one piecewise-sinusoidal current function across the length of the dipole), J.H. Richmond's moment method computer code [19] which utilizes overlapping piecewise-sinusoidal current functions was used for comparison. Consider the case where the dipole arms are tilted by 45° and the arm length is one-quarter wavelength; that is, $\alpha = 45°$ and $l_v = 0.25\lambda$ in Equation (2.40). (Note: these parameters will be used in the theoretical probe model discussed in the next section.) The results are presented in Figure 2-4 for one, three, and five piecewise-sinusoidal current functions or unknowns.

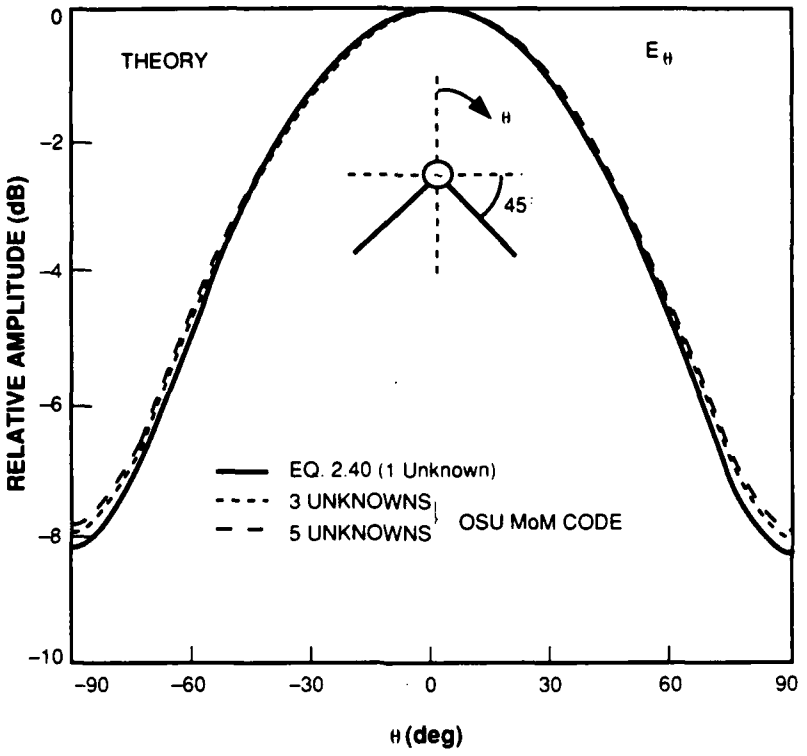

129825-3

Figure 2-4. Comparison of far-field radiation patterns for $\lambda/2$ center-fed V-dipole antenna in free space using Equation (2.40) and Richmond's thin-wire moment method code.

The indication is that one unknown produces a far-field pattern which agrees to within about 0.3 dB of the pattern obtained with five unknowns. This is consistent with other simulations of V-dipole antenna elements [20]; thus, Equation (2.40) is sufficiently accurate for purposes of performing probe compensation in this report.

3. EXPERIMENTAL LOW-SIDELOBE PHASED ARRAY ANTENNA

A precision 32-element linear phased array antenna [21] has been constructed for purposes of developing and evaluating near-field measurement techniques. A photograph of the array is shown in Figure 3-1.

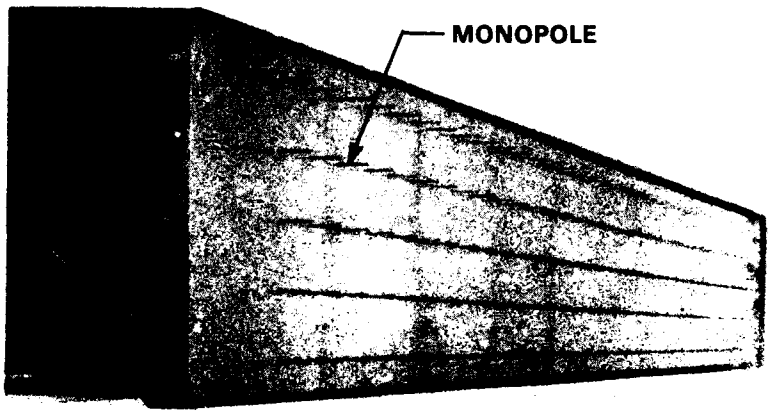

129825-4

Figure 3-1. Photograph of 32-element linear phased array antenna.

The array operates at L-band (1.25 to 1.35 GHz) and consists of coaxially fed monopole antenna elements arranged in a square lattice having 5 rows and 36 columns with spacing equal to 4.3 in. To reduce edge effects, two guard bands of passively terminated elements completely surround the center row of 32 active elements. The passive terminations are 50-ohm resistive loads. The length and diameter of the monopole elements are 2.4 and 0.125 in, respectively. Each monopole consists of a brass rod mounted on a type-N connector. The ground plane dimensions are 24 by 172 in with a flatness which was measured to be within 0.020 in peak. A simplified block diagram of the receive portion of the T/R module is shown in Figure 3-2.

The phase shifter is implemented in the 1100-MHz first local oscillator line. Beginning at a 275-MHz carrier frequency, 0 to 90° phase shift with 12 bits is effected. Next, frequency multiplication by four and filtering is used to generate the 0 to 360° phase controlled 1100-MHz LO. The RF signal is mixed initially down to the 150- to 250-MHz band, and then it is mixed with a 120- to 220-MHz tone down to a fixed 30 MHz. It is here that amplitude control is effected, also with 12 bits. A 40-dB attenuation range is implemented using two cascaded voltage controlled attenuators. Measured amplitude and phase tolerances of these modules were typically less than 0.02 dB and 0.2°, respectively. The slightly nonlinear characteristics of the voltage controlled attenuators and phase shifters require calibration using a microprocessor which was built into each module. All modules were connected to a serial data bus. This bus permitted all modules to simultaneously receive commands from a general-purpose desktop computer. The power combiner (beamformer) is implemented at 30 MHz with an isolation greater than 40 dB between ports.

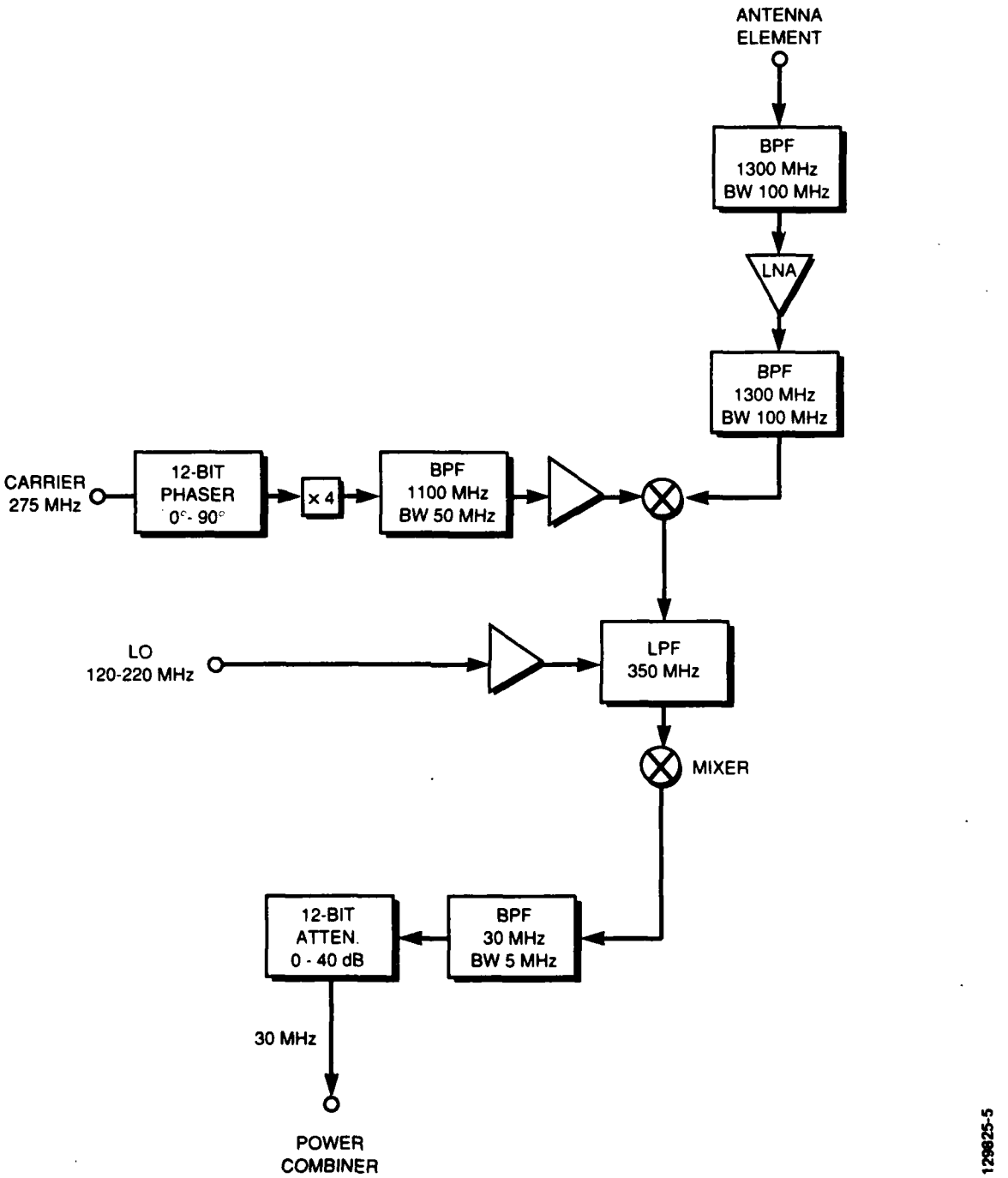

Figure 3-2. Block diagram for receive portion of T/R module.

4. NEAR-FIELD MEASUREMENTS SYSTEM

A linear scanner was built [21] to evaluate the performance of the above phased array antenna. The near-field probe position in the x-direction is determined by a laser range finder and adjusted by means of a stepper motor driven cogged belt. The probe position accuracy is to within 0.002 in of the desired position. For the test antenna, amplitude and phase measurements are made easier and more accurately by the fact that the output of the array is at a 30-MHz intermediate frequency; thus, a low frequency network analyzer can be used to make these measurements with the desired degree of precision.

The near-field probe consists of a standard L-band coaxial to rectangular waveguide transition with the flange removed and surrounded with a 24 by 24-in square sheet of pyramidal anechoic material. The rectangular waveguide (WR-650) inside dimensions are 6.5 by 3.25 in. A photograph of the near-field probe is shown in Figure 4-1. The measured VSWR of this antenna, over the frequency range 1.2 to 1.4 GHz, is less than 1.8:1 as depicted in Figure 4-2. In particular, at 1.3 GHz the VSWR is equal to 1.7:1. Far-field E-plane radiation patterns of the rectangular waveguide near-field probe (with and without the surrounding absorber sheet) were measured on a conventional far-field antenna range. The measured data are shown in Figure 4-3. It is clear that the absorber modifies the free-space pattern shape. All near-field data presented in this report were collected with the absorber/waveguide probe combination. The purpose of the absorber is to reduce reflections that may occur between the test antenna and the near-field probe support arm.

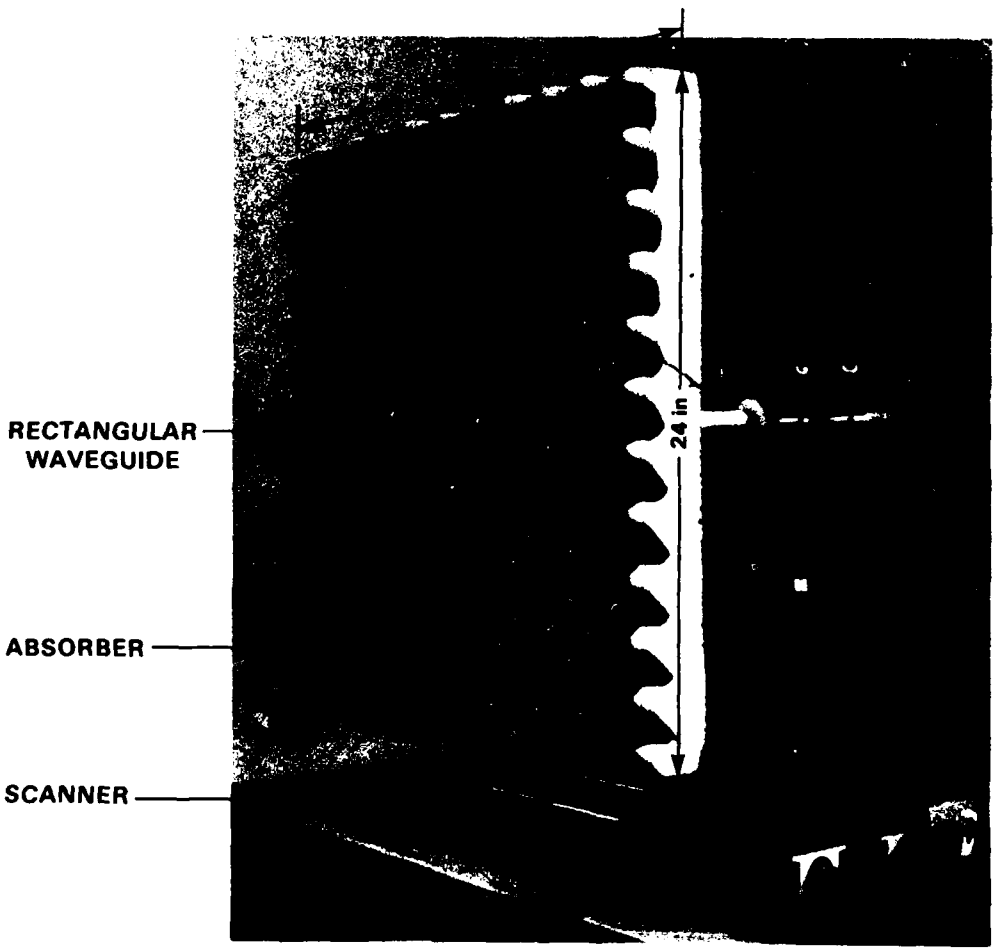

Photograph of rectangular waveguide near-field probe with absorber.

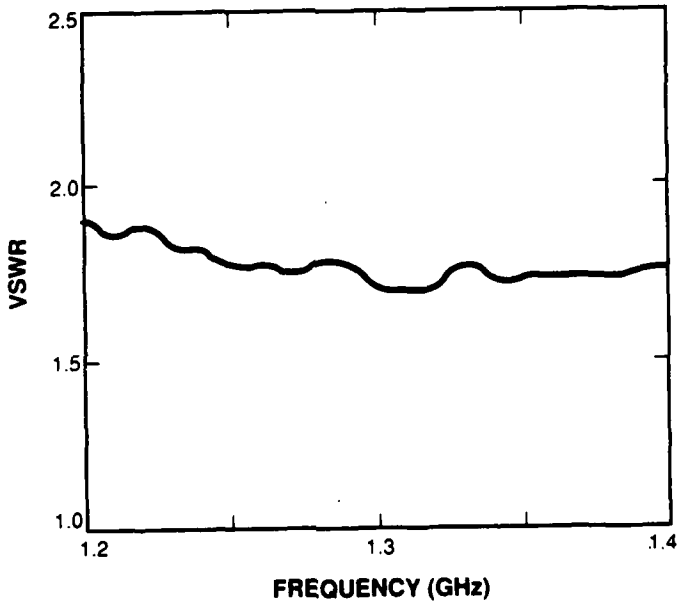

131130-5

Figure 4-2. Measured VSWR for rectangular waveguide near-field probe.

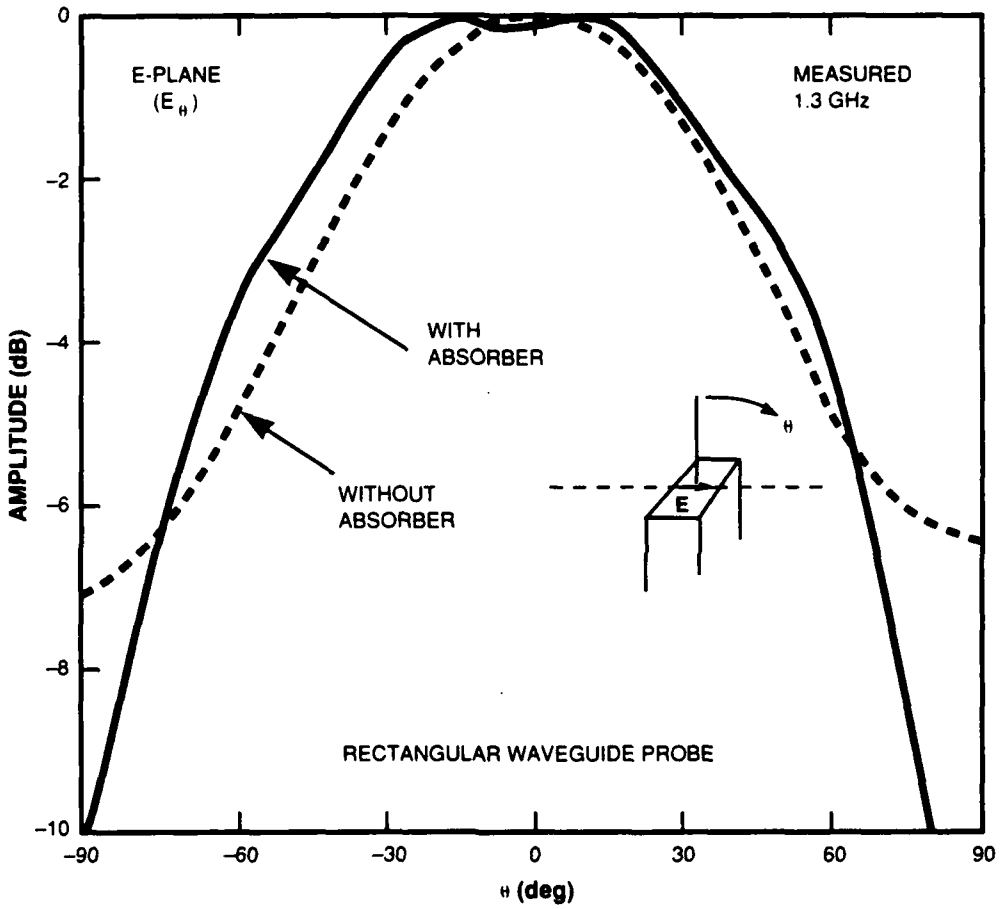

Figure 4-3. Measured far-field patterns for rectangular waveguide near-field probe with and without absorber.

5. RESULTS

5.1 SELECTION OF THEORETICAL PROBE MODEL

As mentioned earlier, the purpose of using a V-dipole probe (with arbitrary arm tilt angle) in the theoretical model is to have flexibility in designing or selecting the probe radiation pattern shape. This flexibility allows the theoretical probe model to closely match the pattern characteristics of the measurement probe. The closed-form far-field pattern for a V-dipole was computed, using Equation (2.40), for various arm tilt angles. Based on the results shown in Figure 5-1, a V-dipole with $\lambda/4$ arm length and 45° arm tilt produces a theoretical pattern that is within 1.0 dB of the measurements (over a $\pm 70°$ field of view) at 1.3 GHz for the open-ended rectangular waveguide probe with absorber. Notice that the $\alpha = 0, 30°$ cases have a substantially larger variation from the measured probe data; thus, the $\alpha = 45°$ V-dipole is selected as the theoretical probe model.

5.2 GRATING LOBE POSITIONS FOR A PHASED ARRAY

The grating lobe positions for a linear array with element spacing D_x and scanned to the angle θ_s are given by [22]

$$k_{x_m} = k \sin \theta_s + \frac{2\pi}{D_x} m; \; m = \pm 1, \pm 2, \cdots \tag{5.1}$$

These grating lobes are nonpropagating provided that they fall within the invisible region where $|k_x| > 2\pi/\lambda$. For an element spacing $D_x = 0.473\lambda$ (corresponding to the experimental array) and scan angle $\theta_s = -30°$, the first grating lobes [$m = \pm 1$ in Equation (5.1)] are located at $k_{x_{-1}} = -16.44$ and $k_{x_1} = 10.16$, both with units of radians per wavelength. Similarly, the second grating lobes are located at $k_{x_{-2}} = -29.71$ and $k_{x_2} = 23.43$. Clearly, these grating lobes fall outside the visible region and do not propagate to the far field. Depending on the near-field distance, these lobes may or may not be present in the resulting plane-wave spectrum.

The largest wavenumber which is produced in the FFT process is found by substituting $K_x = N_x$ in Equation (2.25) with the result

$$k_x^{max} = \frac{\pi}{d_x}.$$

For the theoretical simulations and experimental measurements, a near-field sample spacing of $d_x = 0.141\lambda$, which produces $k_x^{max} = 22.24$, was chosen. This means that, in computing the FFT, any large plane-wave spectrum amplitude components above $|k_x| = 22.24$ will be aliased [23]. For example, the second grating lobe ($m = 2$) at $k_x = 23.43$ will alias to the position $k_x = -21.05$. This is demonstrated in the following section.

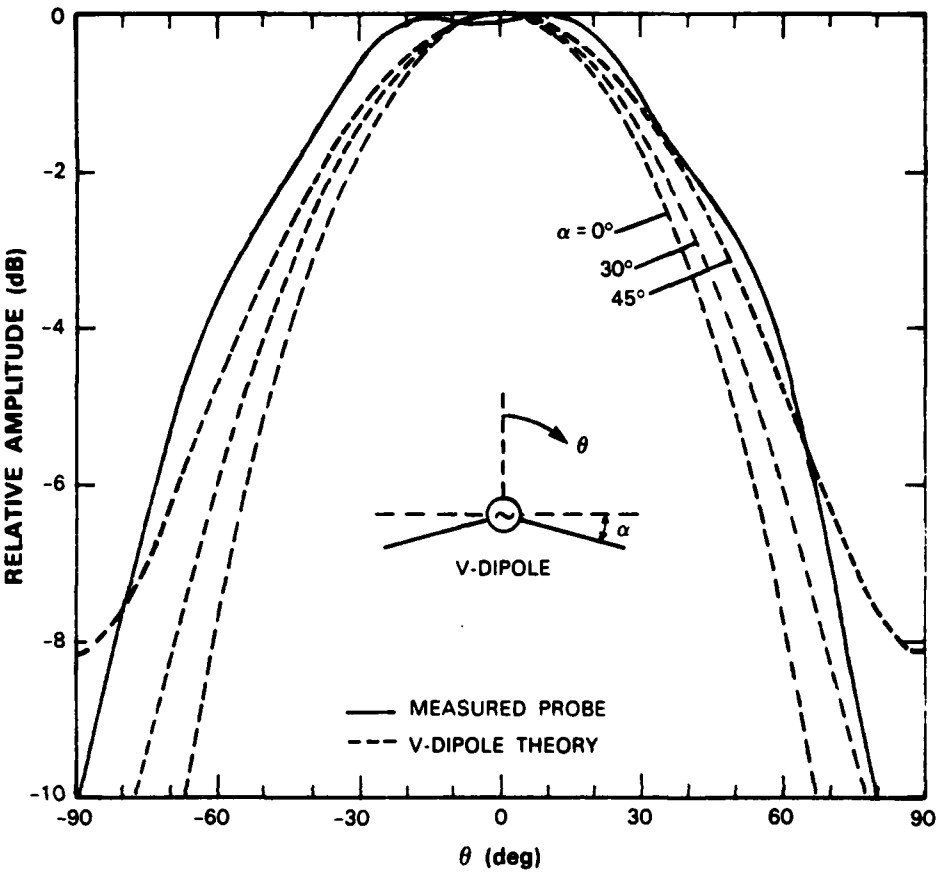

Figure 5-1. Comparison of far-field radiation patterns for theoretical V-dipole antenna with various arm tilt angles and experimental rectangular waveguide near-field probe with absorber.

5.3 FIELD POINT THEORY COMPARED WITH V-DIPOLE PROBE THEORY

The experimental array discussed in chapter 3 was simulated using the moment method formulation presented in chapter 2. The array illumination was assumed to be a 40-dB Taylor taper ($\bar{n} = 10$) with the main beam steered to $\theta_s = -30°$.

A sketch of the 32-element linear test array and near-field scan geometry is given in Figure 5-2. Notice that the shaded elements along the center row form the active linear array, while the unshaded elements form two guard bands with passive terminations (50-ohm resistive). The length of the 32-element active array is 133.3 in. A centerline scan (x variable, $y = 0$) of length 163.02 in was taken at the distance $z_0 = 5$ in. This sampled the near field down to about the 40-dB (or more) level. The number of near-field data samples is 128 and, to evaluate the plane-wave spectrum,

a 2048-point FFT (with zero-filling) is used. At 1.3 GHz, the near-field distance is 0.55λ which implies that the scan is performed in the reactive region. Here, it is expected that nonpropagating grating lobes will be present in the invisible region ($|k_x| > 2\pi/\lambda$) of the plane-wave spectrum.

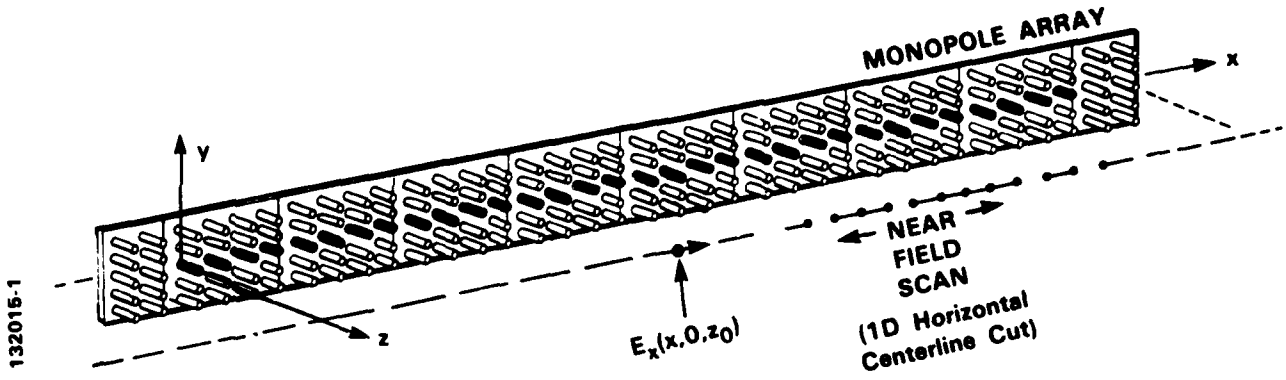

Figure 5-2. Geometry for monopole array and near-field centerline scan. The 32 shaded elements are active and the unshaded elements are passively terminated.

The principal polarization for this array along the centerline scan is the $\hat{x}$ component. For the field point theory, the tangential electric field component $E_x(x, 0, z_0)$ is computed using Equation (2.30), and the plane-wave spectrum component A_x is computed according to Equation (2.7). The far-zone E_θ component is computed based on Equation (2.9). In the case of the V-dipole probe theory, Equation (2.39) is used to compute directly the received voltage $v^x(x, 0, z_0)$ from which Equation (2.15) is implemented to obtain the probe-distorted plane-wave spectrum component A'^x. The probe-compensated E_θ component is then computed according to Equation (2.24).

A comparison of the two theories is now made and the effects of the near-field probe are shown. The near-field amplitude and phase are shown in Figure 5-3 where the field point and dipole theories yield similar results; however, the field point theory has a substantially higher peak-to-peak amplitude ripple (1.0 dB) compared with the V-dipole theory (0.2 dB). The number of ripples, 32, is equal to the number of active array elements. Over the active portion of the phased array, the root mean square (rms) differences between the two theories are 0.74 dB and 8.0°. The ripple amplitude is directly related to the grating lobe amplitude observed in the antenna plane-wave spectrum. Figure 5-4 shows the plane-wave spectrum for both theories. Notice the presence of the expected first grating lobes at $k_x = 10.16$ and $k_x = -16.44$. The field point theory grating lobes are higher than the corresponding V-dipole probe theory lobes; however, the probe theory lobes should be distorted, in amplitude, because of the effect of the V-dipole probe. Presumably, probe compensation of the plane-wave spectrum would produce grating lobes of the correct amplitude; however, this was not of interest here. What is important is the presence of an aliased grating lobe for the field point theory. This is located at the wavenumber $k_x = -21.05$. No such alias occurs for the V-dipole theory. This seems to indicate that evanescent lobes may not be as significant of a problem, in terms of creating aliases or errors in the evanescent and radiating portion of the

plane-wave spectrum, for a V-dipole probe when compared with the field point theory. As will be shown in the next section, the same conclusion can be drawn for a practical waveguide probe.

Next, the transformed far-field patterns, E_θ component, are shown in Figure 5-5. Note that probe compensation has been used in the case of the V-dipole theory, and that the agreement between the two theories is very good.

To show that a centerline scan provides adequate information for the near-field to far-field transformation, Figure 5-6 compares the field point theory transformed pattern with the direct far-field pattern computed using Equation (2.32). Very little differences between the two patterns can be seen, and the differences can likely be attributed to the truncation of the near-field data at the edges of the near-field scan.

5.4 V-DIPOLE PROBE THEORY COMPARED WITH NEAR-FIELD MEASUREMENTS

The purpose of developing the V-dipole probe near-field theory was to be able to make accurate predictions of the behavior of a phased array antenna. In this section, comparisons of the results obtained using theory and experiments are made, and good agreement is achieved.

The experimental 32-element monopole array was calibrated at 1.3 GHz and commanded to steer the main beam to $\theta_s = -30°$ with a 40-dB Taylor taper. A comparison of the near-field measurements and V-dipole probe theory (this is the same theoretical data which was compared with the field point theory) is shown in Figure 5-7. Clearly, the agreement is good, and the rms difference between the theory and measurements is 0.2 dB and 1.5°. The peak-to-peak ripple is 0.5 dB for the measurements compared with 0.2 dB for the theory; thus, the measured grating lobes should be higher than the theoretical grating lobes, and this is the case as the probe-distorted plane-wave spectrum shows in Figure 5-8. The first grating lobes are evident in this figure, and there is no indication of any large aliased grating lobes. The probe-compensated far-field patterns are shown in Figure 5-9 and are generally in good agreement. It should be noted that the theoretical results do not include T/R module quantization or random errors. The average sidelobes are -47.3 dB measured and -46.5 dB theoretical. There is a slight filling-in of the monopole null near $\theta = 0°$ for the measurements, but this is at the –60-dB level.

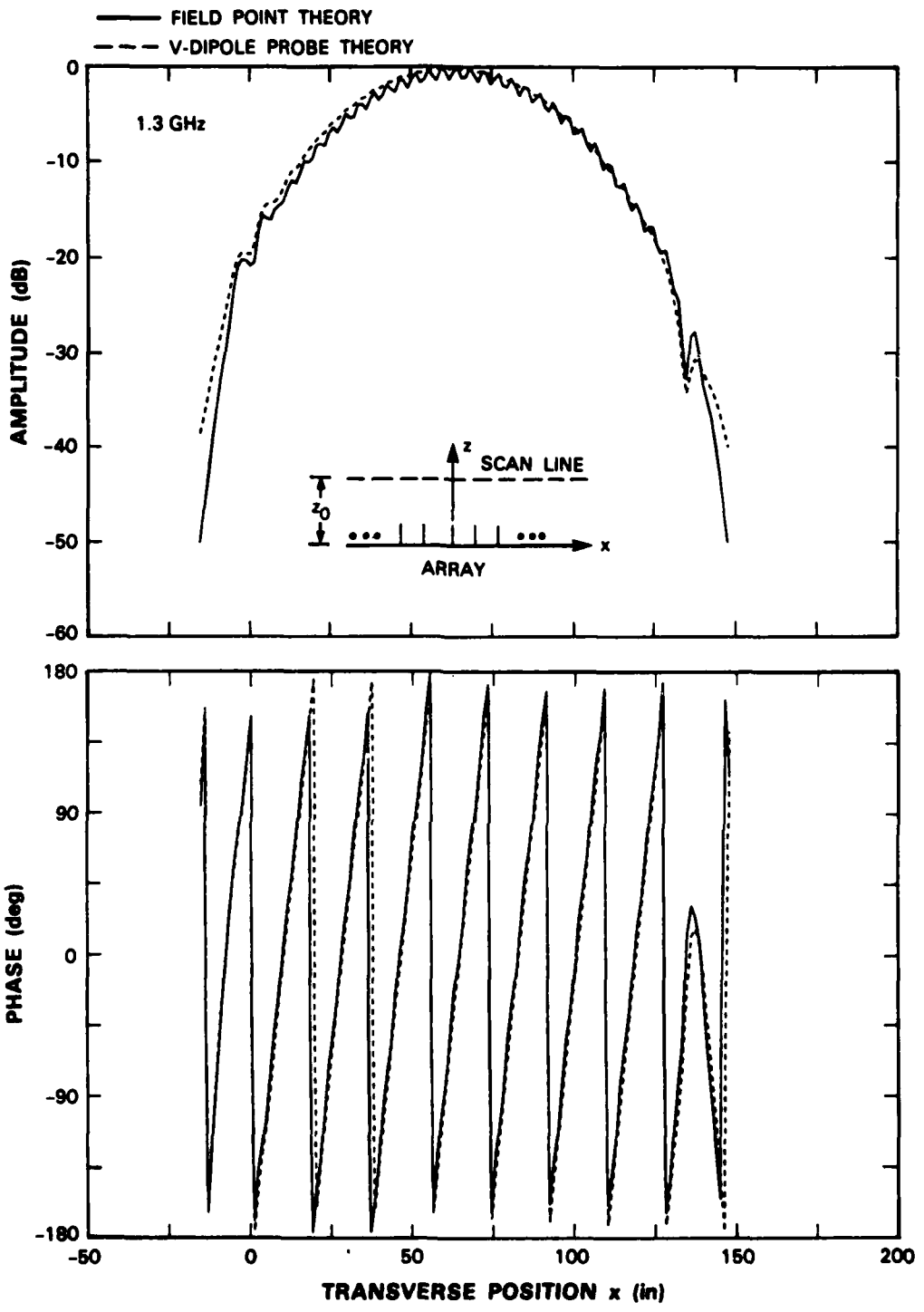

Figure 5-3. Comparison of 32-element monopole array near-zone electric field $E_x(x)$ using the field point theory and the array received voltage $v^x(x)$ due to a V-dipole transmitting antenna using the V-dipole theory. The near-zone data are computed at the distance $z_0 = 0.55\lambda$: (a) amplitude and (b) phase.

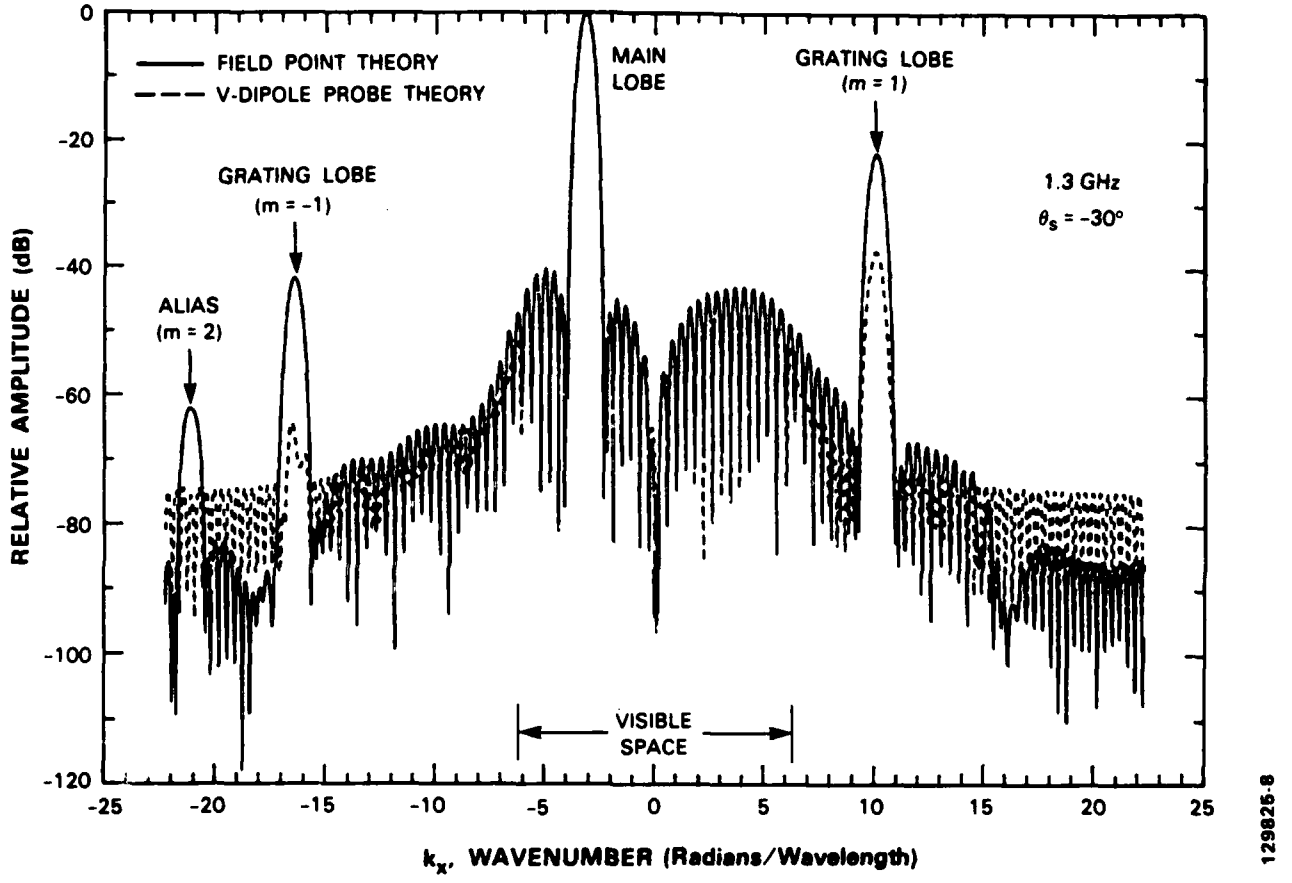

Figure 5-4. Comparison of 32-element monopole array field point theory plane-wave spectrum $A_x(k_x, z_0 = 0.55\lambda)$ and V-dipole theory probe-distorted plane-wave spectrum $A'^x(k_x, z_0 = 0.55\lambda)$.

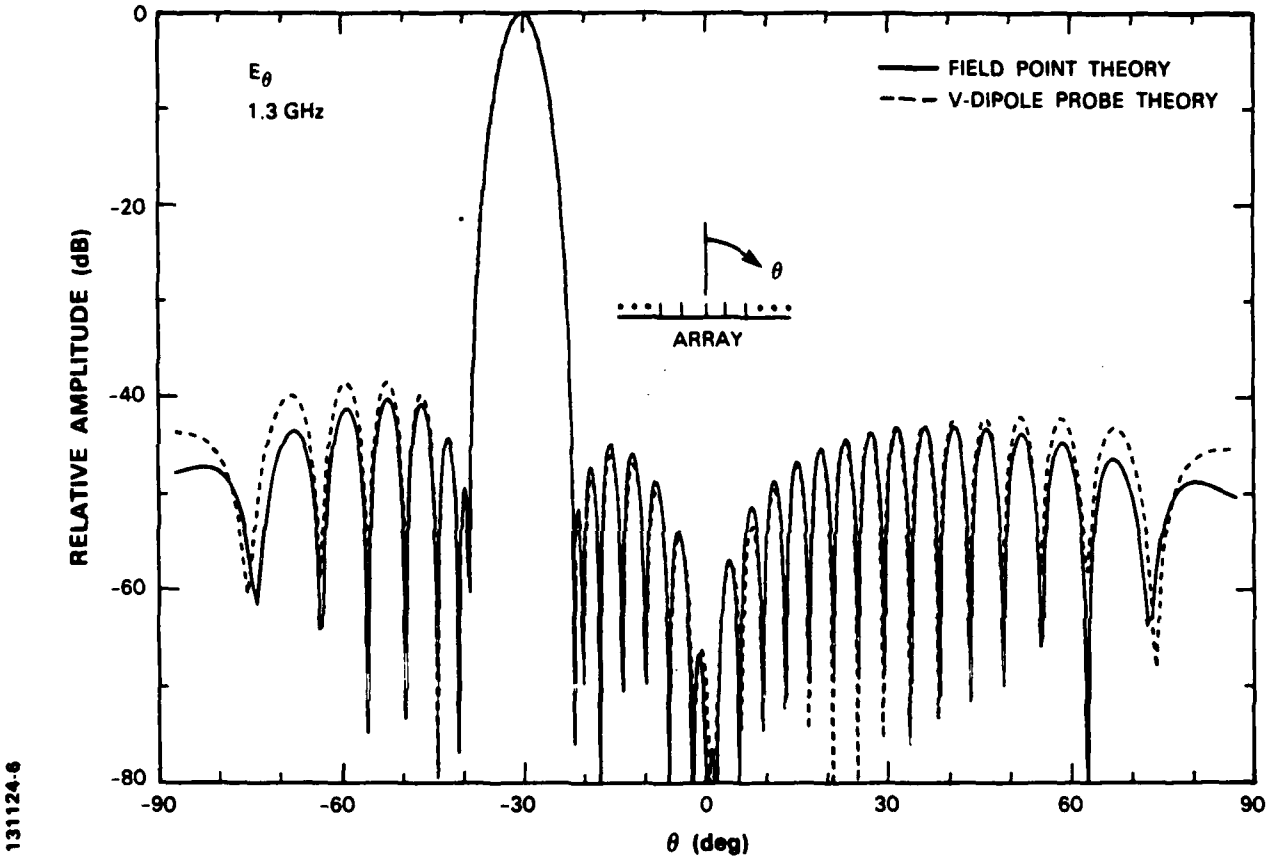

Figure 5-5. Comparison of 32-element monopole array far-field patterns computed using the field point theory and the V-dipole probe theory.

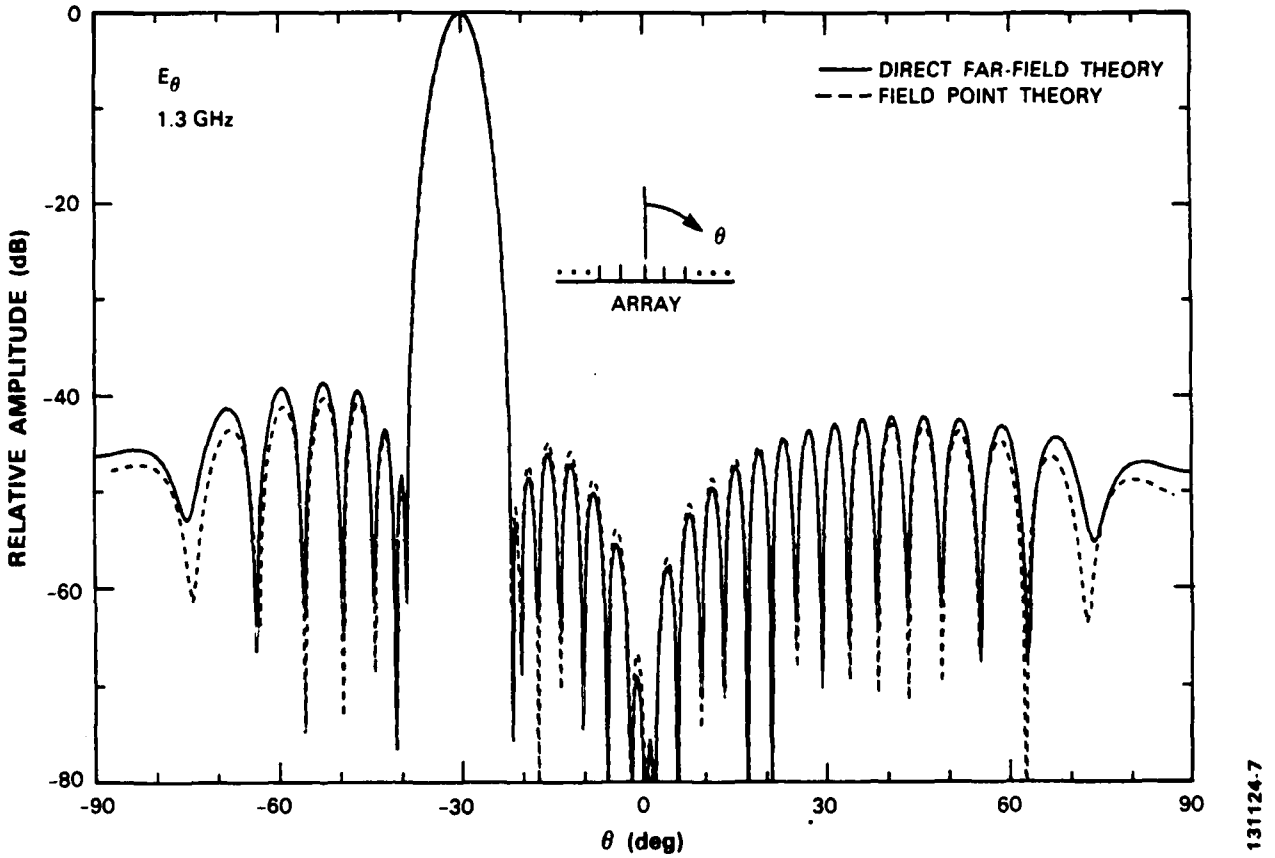

Figure 5-6. Comparison of 32-element monopole array far-field patterns based on the field point theory [Equation (2.30)] and the direct method [Equation (2.32)].

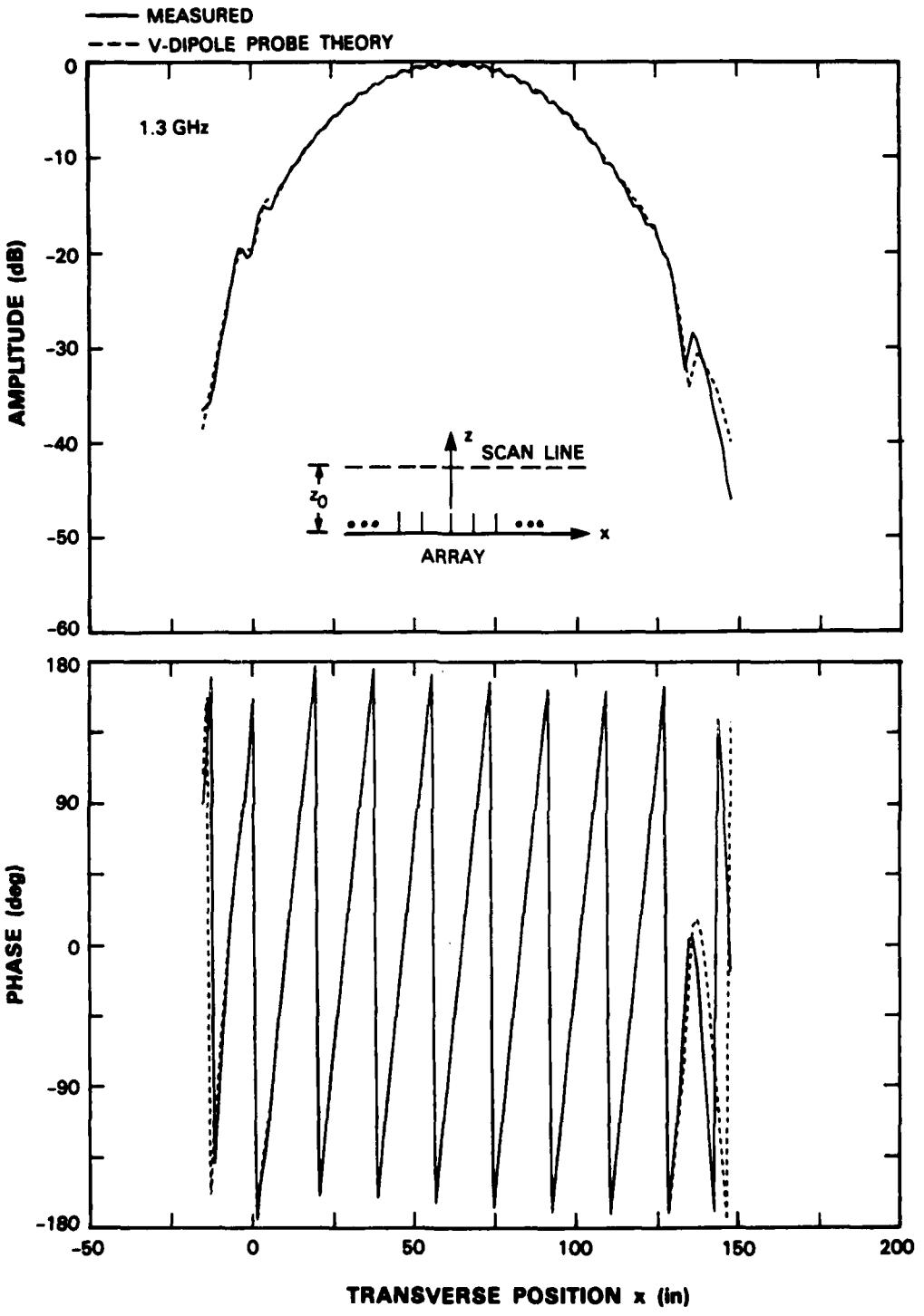

131861-2

Figure 5-7. Comparison of measured and theoretical near-zone received voltage for the 32-element monopole array. The measurement probe is a open-ended rectangular waveguide surrounded with anechoic material. The theoretical probe is a V-dipole. The near-zone distance is $z_0 = 0.55\lambda$: (a) amplitude and (b) phase.

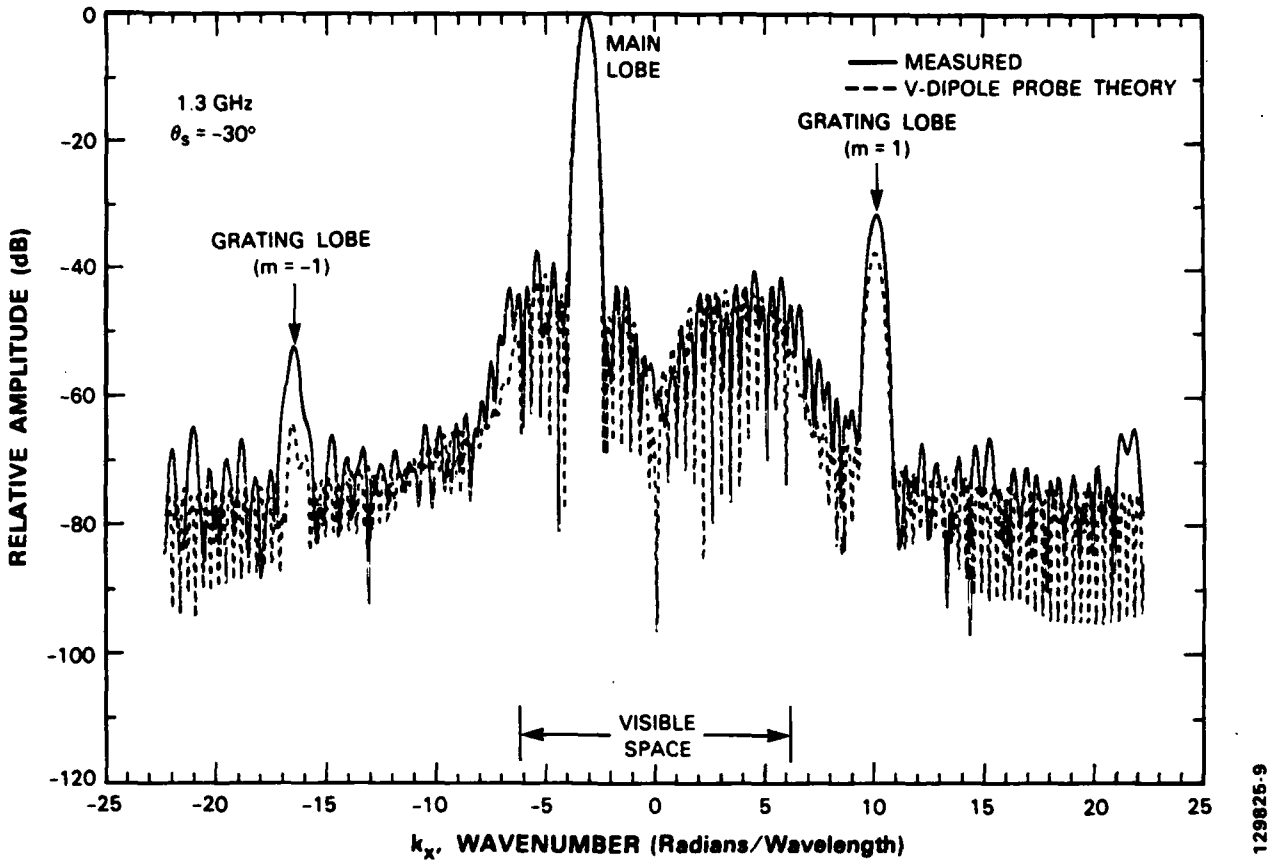

Figure 5-8. Comparison of 32-element monopole array probe-distorted plane-wave spectrum based on near-zone measurements and V-dipole probe theory. The near-zone distance is $z_0 = 0.55\lambda$.

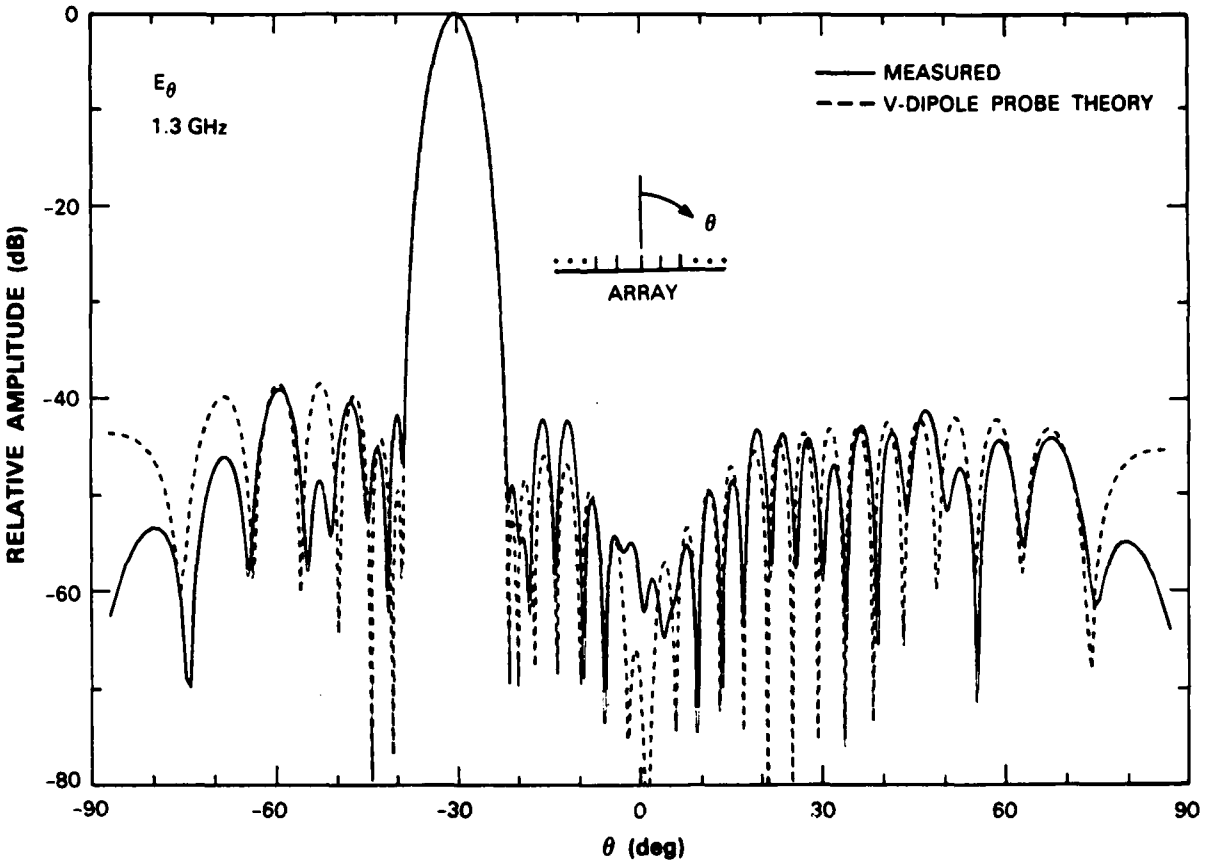

Figure 5-9. Comparison of 32-element monopole array probe-compensated far-field patterns based on near-zone measurements and V-dipole probe theory. The near-zone distance is $z_0 = 0.55\lambda$. The theory does not include T/R module quantization or random errors.

6. CONCLUSION

The technique of planar near-field scanning, with and without probe compensation, has been investigated theoretically using the method of moments, to determine the characteristics of phased array antennas. A monopole phased array antenna has been analyzed using a field point theory where the near-zone electric field of the antenna is computed. The near field is transformed, via the plane-wave spectrum, to a far-field pattern. Probe compensation is not required in this case. A probe theory, where the array near-zone received voltage due to a V-shaped dipole radiating antenna is computed, has also been presented. For the V-dipole theory, probe compensation was implemented using a closed-form expression for the far-field pattern of the V-dipole. The usefulness of centerline scanning in determining the far-field pattern for a linear array has been demonstrated numerically by comparing a direct far-field calculated pattern with a near-field to far-field calculated pattern.

The design and construction of an experimental low-sidelobe monopole phased array antenna has been described. Simulations of this antenna using both theories have been made. The simulations indicate that evanescent (nonpropagating) grating lobes, in the plane-wave spectrum, have a lower amplitude when observed by a V-dipole probe compared with those observed by the field point theory. Adjusting the tilt angle of the V-dipole arms allowed the V-dipole far-field pattern to match approximately the far-field pattern of an experimental rectangular waveguide probe surrounded with absorber. It was shown that the V-dipole probe theory can accurately model the observed experimental performance of a monopole array. The theory can be applied readily to other type of array thin-wire elements such as dipoles.

REFERENCES

1. D.T. Paris, W.M. Leach, and E.B. Joy, "Basic theory of probe-compensated near-field measurements," *IEEE Trans. Antennas Propag.* AP-26, 3, 373-379 (1978).

2. E.B. Joy, W.M. Leach, G.P. Rodrigue, and D.T. Paris, "Applications of probe-compensated near-field measurements," *IEEE Trans. Antennas Propag.* AP-26, 3, 379-389 (1978).

3. A.D. Yaghjian, "An overview of near-field antenna measurements," *IEEE Trans. Antennas Propag.* AP-34, 1, 30-45 (1986).

4. E.S. Gillespie, (guest ed.), "Special issue on near-field scanning techniques," *IEEE Trans. Antennas Propag.* AP-36, 6 (1988).

5. A.C. Newell and M.L. Crawford, "Planar near-field measurements on high performance array antennas," National Bureau of Standards Report No. NBSIR 74-380 (1974).

6. E.B. Joy and D.T. Paris, "Spatial sampling and filtering in near-field measurements," *IEEE Trans. Antennas Propag.* AP-20, 3, 253-261 (1972).

7. J.H. Wang, "An examination of the theory and practices of planar near-field measurement," *IEEE Trans. Antennas Propag.* AP-36, 6, 746-753 (1988).

8. J.D. Hanfling, G.V. Borgiotti, and L. Kaplan, "The backward transform of the near field for reconstruction of aperture fields," *1979 IEEE AP-S Symposium Digest, Vol. 2*, IEEE, New York, 764-767.

9. G. Borgiotti, "Fourier transforms method in aperture antennas problems," *Alta Frequenza* 32, 11, 808-816 (1963).

10. D.R. Rhodes, *Synthesis of Planar Antenna Sources*, Oxford University Press (1974).

11. W.L. Stutzman and G.A. Thiele, *Antenna Theory and Design*, Wiley (1981).

12. D. Castello and B.A. Munk, "Tables of mutual impedance of identical dipoles in echelon," The Ohio State University, ElectroScience Laboratory, Technical Report 2382-1 (17 October 1967) DTIC AD-822013.

13. A.J. Fenn, "Theoretical and experimental study of monopole phased array antennas," *IEEE Trans. Antennas Propag.* AP-33, 10, 1118-1126 (1985).

14. S.A. Schelkunoff, *Electromagnetic Waves*, D. Van Nostrand Co., Inc., (1943), pp. 370-371.

15. I.J. Gupta and A.A. Ksienski, "Effect of mutual coupling on the performance of adaptive arrays," *IEEE Trans. Antennas Propag.* AP-31, 5, 785-791 (1983).

16. A.J. Fenn, "Moment method analysis of near field adaptive nulling," *IEE Sixth International Conf. on Antennas and Propag., ICAP 89 Proceedings*, 4-7 April 1989, pp. 295-301.

17. J.H. Richmond and N.H. Geary, "Mutual impedance of nonplanar-skew sinusoidal dipoles," *IEEE Trans. Antennas Propag.* AP-23, 3, 412-414 (1975).

18. S.A. Schelkunoff and H.T. Friis, *Antennas, Theory and Practice*, Wiley, (1952), pp. 499-501.

19. J.H. Richmond, "Radiation and scattering by thin-wire structures in a homogeneous conducting medium (computer program description)," *IEEE Trans. Antennas Propag.* AP-22, 2, 365 (1974).

20. A.J. Fenn, "Element gain pattern prediction for finite arrays of V-dipole antennas over ground plane," *IEEE Trans. Antennas Propag.* AP-36, 11, 1629-1633 (1988).

21. H.M. Aumann and F.G. Willwerth, "Near-field testing of a low-sidelobe phased array antenna," *Proceedings of the Antenna Measurement Techniques Association 1987 Meeting*, 28 September – 2 October 1987, pp. 3-7.

22. R.C. Hansen, (ed.), *Microwave Scanning Antennas, Volume II, Array Theory and Practice*, Peninsula Publishing, (1985), pp. 199-208.

23. A.C. Newell, "Error analysis techniques for planar near-field measurements," *IEEE Trans. Antennas Propag.* AP-36, 6, 754-768 (1988).

REPORT DOCUMENTATION PAGE

Form Approved
OMB No. 0704-0188

1. AGENCY USE ONLY *(Leave blank)*	2. REPORT DATE	3. REPORT TYPE AND DATES COVERED
	14 February 1990	

4. TITLE AND SUBTITLE

Low-Sidelobe Phased Array Antenna Characteristics Using the Planar Near-Field Scanning Technique: Theory and Experiment

5. FUNDING NUMBERS

F19628-90-C-0002

6. AUTHOR(S)

Alan J. Fenn, Herbert M. Aumann, and Frank G. Willwerth

7. PERFORMING ORGANIZATION NAME(S) AND ADDRESS(ES)

MIT, Lincoln Laboratory
P.O. Box 73
Lexington, MA 02173-9108

8. PERFORMING ORGANIZATION REPORT NUMBER

Technical Report 870

9. SPONSORING/MONITORING AGENCY NAME(S) AND ADDRESS(ES)

HQ AF Space Systems Division SD/XR
Los Angeles AFB, CA 90009-2960

10. SPONSORING/MONITORING AGENCY REPORT NUMBER

ESD-TR-89-235

11. SUPPLEMENTARY NOTES

None

12a. DISTRIBUTION/AVAILABILITY STATEMENT

Approved for public release; distribution is unlimited.

12b. DISTRIBUTION CODE

13. ABSTRACT *(Maximum 200 words)*

Characteristics of a low-sidelobe phased array antenna are investigated using the technique of planar near-field scanning. The theory associated with the planar near-field scanning technique, with and without probe compensation, is reviewed and an application of the theory is made. The design of an experimental low-sidelobe phased array antenna consisting of monopole elements which are corporate-fed using high precision transmit/receive modules is described. Accurate array radiation patterns are obtained both theoretically and experimentally using centerline scanning at less than one wavelength distance from the antenna. The effects of the antenna probe on the array near-field pattern, plane-wave spectrum, and far-field pattern are demonstrated theoretically using a method of moments numerical simulation. Comparisons of the array theoretical near-zone electric field and array received voltage due to a V-dipole near-field transmitting probe are made. It is shown that a V-dipole theoretical probe antenna can accurately model a practical near-field measurement probe consisting of an open-ended rectangular waveguide surrounded with anechoic material.

14. SUBJECT TERMS			15. NUMBER OF PAGES
phased array antennas	plane-wave spectrum	waveguide probe	50
planar near-field scanning	monopole array	antenna testing	16. PRICE CODE
low sidelobes	V-dipole probe		

17. SECURITY CLASSIFICATION OF REPORT	18. SECURITY CLASSIFICATION OF THIS PAGE	19. SECURITY CLASSIFICATION OF ABSTRACT	20. LIMITATION OF ABSTRACT
Unclassified	Unclassified	Unclassified	